

NATIONAL RADIO ASTRONOMY OBSERVATORY
Green Bank, West Virginia

PRINCIPAL CONSIDERATIONS OF RADIOASTRONOMICAL
OBSERVATIONS AT VERY HIGH FREQUENCIES

Peter G. Mezger

MARCH 1964

PRINCIPAL CONSIDERATIONS OF RADIOASTRONOMICAL OBSERVATIONS AT VERY HIGH FREQUENCIES

Peter G. Mezger

Introduction

Radioastronomical observations in the cm-wave region ($10 \text{ cm} \geq \lambda \geq 1 \text{ cm}$) have already yielded important results, especially concerning the spectrum and the polarization of radio sources, the investigation of H_{II} -regions, and the thermal radiation of the moon and the planets. The results obtained until now in the mm-wave region ($10 \text{ mm} \geq \lambda \geq 1 \text{ mm}$) are not very numerous, but it is obvious that — apart from the sun and the moon — the observation of the planets will be the principal task in this wavelength region. As far as the sub-mm-wave region ($1 \text{ mm} \geq \lambda \geq 30 \mu\text{m}$) is concerned, only in the past few years has an effort been made to improve receiver techniques. Very little is therefore known concerning the transparency of the atmosphere and the most intense cosmic radiation sources in this wavelength region.

In this report we limit ourselves to the cm- and mm-wavelength region. In section I the influence of the atmosphere and the concept of antenna temperature will be discussed. In section II the observation instruments are reviewed, with special emphasis on the antennas available or scheduled at the NRAO. The present state of radio (or coherent) receiver technique is summarized with an outlook as to what improvement may be expected within the next two years. It is shown that the minimum detectable radiation power is limited by the atmosphere rather than by the receiver noise. In section III the possibility of radioastronomical observations in the cm- and mm-wave region are discussed. In particular, the antenna temperatures of the strongest radio sources, the moon, and the planets have been calculated.

These results, in conjunction with our estimates of the influence of the atmosphere, may serve as a base for the following decisions:

1. At which wavelengths shall observations be made?
2. Which type of receiver shall be chosen?
3. Which radioastronomical observation programs can be started with the available antennas?

I. 1. The Influence of the Atmosphere

The radiation of an extraterrestrial radio source is deviated and attenuated while traveling through the atmosphere. This second effect is known as the "extinction" of the atmosphere. The extinction may be caused by absorption lines of the gaseous components of the atmosphere as well as by scattering. In the cm- and mm-wavelength range and under good observing conditions (meaning no condensed water vapor in the atmosphere), the scattering effect is negligible.

Measurements of the atmospheric refraction have been made over the wavelength range from 20 to 0.4 cm. The results are plotted in figure 1. As may be seen from this diagram, refraction seems to be independent of frequency throughout the microwave region.

The attenuation at a frequency ν is described completely by the transmission coefficient p at zenith distance $z = 0$. If $I_{\text{extraterr}}$ is the intensity of a radio source outside the atmosphere, the corresponding intensity of the source observed at the zenith distance z is

$$(1) \quad I(z) = I_{\text{extraterr}} p^{F(z)}$$

For zenith distances $z < 80^\circ$ $F(z) = \sec z$. For higher values z the rigorous air mass function has to be taken. The attenuation, or more precisely the loss, of the atmosphere is then $1 - p^{F(z)}$, and consequently the radiation temperature of the atmosphere is given by*

$$(2) \quad T_b(z) = T_{\text{at}} [1 - p^{F(z)}]$$

as long as the Rayleigh-Jeans approximation holds.

T_{at} means a weighted value of all layers of the atmosphere, which is with a fairly good approximation independent of the zenith distance.

* It is not known if this relation holds throughout the mm- and submm-region. Westphal has shown [34] that in the infrared window (8-14 μm) an increase in absorption can be associated with a decrease in sky temperature, and that the sky temperature is considerably higher than would be expected from equation (2).

$T_{at} = 265 \text{ }^\circ\text{K}$ is a good assumption under normal meteorological conditions. In the wavelength range here considered the attenuation of the atmosphere is caused by absorption lines of the water vapor and the oxygen. The resulting absorption of the atmosphere depends not only on the total amount of water vapor and oxygen in the line-of-sight but also on the temperature and pressure in the different layers of the atmosphere. The widths of the absorption lines become smaller with increasing altitude.

The distribution of oxygen varies only slowly with the altitude, whereas the water vapor distribution depends very strongly on the altitude. The amount of precipitable water at an altitude of 4 km, e. g. , only $7.3 \cdot 10^{-2}$ times the amount at sea level. An observatory site at a very high altitude, say 4 km, therefore can improve the observing conditions considerably only as far as the influence of water vapor is concerned,

The transmission coefficient for the cm- and mm-wave region has been calculated by R. Menon [2] for the altitude of Green Bank (823 m) and for the amounts of precipitable water $w_v = 2.1 \text{ cm}$ and 0.37 cm , respectively, which values correspond to the best and worst observing conditions (apart from cloudy sky) at this place. The curves (fig. 2) have been taken from this paper [2] on the attenuation of the atmosphere. The curves give the negative logarithmic value of the transmission coefficient $-\log p$ as a function of frequency. For small values of p an approximate relation between p and $\log p$ may be obtained using a series expansion

$$(3) \quad 1 - p = \frac{\log p}{0.4343}$$

From figure 2 we get the preferred frequency bands for radioastronomical observations in the cm- and mm-wave region. The first water vapor absorption line which occurs at about 21.5 GHz is not a very serious limitation. Nevertheless, one will try to avoid this line. So, we get the observation bands listed in the following table.

TABLE 1

Center frequency f_o	Bandwidth B	Loss due to atmospheric absorption	
		$1 - p_{\min}$ ($w_v = 3.7$ mm)	$1 - p_{\max}$ ($w_v = 2.1$ cm)
≤ 15 GHz*		10^{-2} *	$3.5 \cdot 10^{-2}$ *
35 GHz	16 GHz***	$3.0 \cdot 10^{-2}$ **	$7.8 \cdot 10^{-2}$ **
85 GHz	30 GHz	$6.9 \cdot 10^{-2}$ **	$1.8 \cdot 10^{-1}$ **
150 GHz	35 GHz	$5.3 \cdot 10^{-2}$ **	$3.4 \cdot 10^{-1}$ **
250 GHz	90 GHz	$4.8 \cdot 10^{-2}$ **	$6.0 \cdot 10^{-1}$ **

* At upper band limit.

** At band center.

*** B = 16 GHz is the bandwidth defined by technical limitations.

The next window in the atmosphere occurs at about 350 GHz and has a useful bandwidth of only 20 GHz. So it seems obvious that the technical effort should be concentrated to the four windows between 35 and 250 GHz.

Until now we have considered only average values of atmospheric refraction and extinction. The accuracy of radioastronomical observations, however, is limited rather by the time variations of refraction and extinction, which in the optical astronomy are referred to as "seeing" and as "scintillation", respectively.

Seeing means that the image of a point source moves at random in the focal plane. The RMS deviations in the optical window are in the order of 0.3" to 1.2" for not too bad observing conditions. In the radio window the "seeing problem" has never been considered for observations with single dishes, since the diffraction limit and pointing accuracy of the radio telescopes are probably order of magnitudes below the seeing limit. In a short paper Drake [3] has mentioned that positions of radio sources have been measured with an accuracy of 3".* A review of phase fluctuation measurements

* From this result and from the fact that the average refraction at optical and radio wavelengths is approximately the same, it may be concluded that single-dish "seeing" is not much worse at radio wavelength.

has been given by Keen [4]. A more extensive treatment of previous experimental work on optical- and radioastronomical seeing is in preparation [5].

Scintillation is a much more serious problem for radioastronomical observations with single dishes, and will probably set an ultimate limit on the minimum detectable radiation power. As has been pointed out by Orhaug [6], scintillation in the microwave region is probably caused by fluctuations of the water vapor in the atmosphere. In the optical region scintillation causes only a random amplitude modulation of the radiation which results in an increased noise. In the microwave region the scintillation causes additionally a fluctuation of the atmospheric radiation.** Orhaug and later Venugopal [7] investigated the sky fluctuations at 8 GHz at the NRAO. Since they did not discriminate between good observing conditions (clear sky) and cloudy or rainy days, their results cannot be used to determine the ultimate limitation due to sky temperature fluctuations. Measurements with a maser at 5 GHz have shown, however, that under fairly good observing conditions the sky temperature fluctuations do not exceed 0.05 °K. We may now assume that these fluctuations are only caused by water vapor; then the fluctuations will be proportional to the attenuation due to water vapor. At 5 GHz and for the altitude of Green Bank the ratio between the water vapor attenuation for the worst case ($w_v = 2.1$ cm) and for the best case ($w_v = 0.37$ cm) is about 11. We may conclude, therefore, that the RMS sky temperature fluctuations are $\sqrt{11 \cdot 0.05} = 0.165$ °K and $0.05/\sqrt{11} = 0.015$ °K, respectively. By multiplying these values with the factor $b(\nu)/b(5 \text{ GHz})$, where b is the attenuation due to water vapor, we have calculated the curves in figure 3. At an altitude of about 4 km (which corresponds to the High Altitude Observatory in Boulder, Colorado) the amount of precipitable water is only 0.17 times the amount of precipitable water at Green Bank. By multiplying the fluctuation temperatures for Green Bank with this factor we obtain a rough estimate of the improvement of observation conditions due to the lower water vapor content of the atmosphere.

** Contrary to the predictions of Silver and Weaver [8], the effect of backscattering of thermal radiation from the earth is negligible, except from water drops. The radiation of the sun, however, either scattered in the main lobe or radiating in a sidelobe of the antenna, often limits sensitive observations to the night time.

It should be kept in mind, however, that the curves in figure 3 represent the extrapolation of one single experimental value over two order of magnitudes in frequency and one order of magnitude in water vapor content in the atmosphere. Consequently, the result can give only an order of magnitude estimate of the expected sky temperature fluctuations in the cm- and mm-wavelength region. Further experimental investigations are very important.

I.2. The Concept of Antenna Temperature

There are two major problems in connection with the concept of antenna temperature at very high frequencies: (a) At low temperatures Planck's law may no longer be replaced by Rayleigh-Jeans law and (b) the measurement of the total flux or of the radiation temperature of radio sources becomes more complicated since the diameter of the sources may be several times the HPBW of the antenna.

Let us first consider point (a). An antenna with the solid angle Ω which is pointed to an unpolarized radio source with the solid angle Ω_s receives the power per Hz bandwidth $P_\nu = AB_\nu \Omega_s$. The power per Hz radiated in the solid angle 1 steradian is in the case of a thermal source given by Planck's law $B_\nu = \frac{2h\nu^3}{C^2} \frac{1}{e^{h\nu/kT} - 1}$. By using the known relation between the effective area A and the solid angle Ω of an antenna $A = \lambda^2/\Omega$ we obtain

$$(4) \quad P_\nu = \frac{\Omega_s}{\Omega} \frac{h\nu}{e^{h\nu/kT} - 1} \approx \frac{\Omega_s}{\Omega} kT$$

The Rayleigh-Jeans approximation of Planck's law holds with an accuracy of better than 1 percent for $\frac{T}{^\circ\text{K}} \geq \frac{\nu}{\text{Hz}} 4.8 \cdot 10^{-10}$. From equation (4) and thermodynamical considerations Nyquist's formula for the available power per Hz of a resistor at a temperature T follows: $P_\nu = h\nu/(\exp \{ h\nu/kT \} - 1)$. For $\lambda \geq 1$ mm the limiting temperature for the application of the Rayleigh-Jeans formula is about 150 °K. This means that the notation of an antenna temperature of, for example, 10 °K becomes ambiguous at this wavelength. Since the system noise temperatures of all radio telescopes in the range $\lambda \geq 1$ mm will be higher than the temperature limit for the application of the

Rayleigh-Jeans law this ambiguity can be avoided by defining the antenna temperature T_A as the corresponding increase of the system noise temperature. Careful receiver calibration is then required; a load cooled with liquid nitrogen is not a useful calibration source at $\lambda = 1$ mm. The relation between antenna temperature T_A and radiation temperature T_s of the source is given by

$$(5) \quad T_A = \frac{\Omega_s}{\Omega} \frac{h\nu}{k} \frac{1}{e^{h\nu/kT_s} - 1}$$

Fortunately, in the wavelength region $\lambda \geq 1$ mm, this problem arises only in a few cases of cool planets, whose solid angles Ω_s are well known, however (see section III. 3).

To investigate the problem mentioned as point (b), we consider the antenna convolution integral. As long as the spherical coordinates ϕ, φ can be replaced by the rectangular coordinates ξ, η this integral can be written in the form

$$(6) \quad T_A(\xi, \eta) = \frac{\eta_B}{\Omega_m} \iint_{-\infty}^{+\infty} f_m(\xi - \xi'; \eta - \eta') T_s(\xi', \eta') d\xi' d\eta'$$

with the antenna main beam pattern f_m and a distribution $T_s(\xi', \eta')$ of the radiation temperature of the radio source. If the apparent source diameter Θ_s is smaller or in the range of the HPBW Θ_A of the antenna, the gaussian approximation for the main beam can be used and the antenna solid angle can be expressed as $\Omega = \frac{\Omega_m}{\eta_R} (1 - \beta_m)$

$$= \frac{\Omega_m}{\eta_B}$$

Here $\Omega_m = 1.133 \Theta_A^2$ the main beam solid angle

β_m = the main beam stray factor

η_R = the radiation efficiency

$\eta_B = \eta_R (1 - \beta_m)$ = the beam efficiency of the antenna.

If the solid source angle Ω_s is very small as compared to the antenna solid angle Ω_A , one obtains the well known relations between antenna temperature T_A , radiation temperature T_s and flux density S_ν of the radio source.

$$(7a) \quad T_A = \frac{\Omega_s}{\Omega_A} \eta_B T_s$$

$$(7b) \quad S_\nu = \frac{2kT_A}{A} = \frac{2kT_A}{\lambda^2 \eta_B} \Omega_m$$

$$\left. \begin{array}{l} (7a) \\ (7b) \end{array} \right\} \Omega_s \ll \Omega_A$$

with A the effective antenna area. In the case of an extended radio source a very general relation for flux density and radiation temperature may be obtained from the convolution integral equation (6)

$$(8a) \quad \iint_{-\infty}^{+\infty} T_A(\xi, \eta) d\xi d\eta = \eta_B \iint_{-\infty}^{+\infty} T_s(\xi, \eta) d\xi d\eta$$

$$(8b) \quad S = \frac{2k}{\lambda^2 \eta_B} \iint_{-\infty}^{+\infty} T_A(\xi, \eta) d\xi d\eta$$

If the source diameter is smaller than the HPBW of the antenna but not so small that it can be neglected, one generally assumes a certain source distribution $T = T_s \psi(\xi, \eta)$. The distribution function is normalized so that $\psi_{\max} = 1$; consequently T_s is the maximum brightness temperature of the source. The most frequently used distributions are

$$(9a) \quad \text{the disk distribution } \psi(\xi, \eta) = \begin{cases} 1 & \text{for } \sqrt{\xi^2 + \eta^2} \leq R \\ 0 & \text{elsewhere} \end{cases}$$

and the Gaussian distribution

$$(9b) \quad \psi(\xi, \eta) = \exp \left\{ -\frac{\xi^2}{(0.6 \Theta_s)^2} - \frac{\eta^2}{(0.6 \Theta_s)^2} \right\}$$

Defining then a modified solid source angle

$$(10) \quad \Omega_s' = \iint_{-\infty}^{+\infty} f(\xi', \eta') \psi(\xi', \eta') d\xi' d\eta' \leq \Omega_s = \iint_{-\infty}^{+\infty} \psi(\xi', \eta') d\xi' d\eta'$$

which is always smaller or equal to the real source solid angle Ω_s the expressions for antenna temperature and flux density can be rewritten in the form

$$(11a) \quad T_A = \frac{\eta_B}{\Omega_m} T_s \Omega_s'$$

$$(11b) \quad S_\nu = \frac{2kT_A}{\eta_B \lambda^2} \frac{\Omega_m \Omega_s}{\Omega_s'}$$

Our experience has shown that a well focused antenna can with a very high accuracy be approximated by the Gaussian function

$$(12a) \quad f_m = \exp \left\{ -\frac{\xi^2}{(0.6 \Theta_A)^2} - \frac{\eta^2}{(0.6 \Theta_A)^2} \right\}$$

with the corresponding main beam solid angle

$$(12b) \quad \Omega_m = 1.133 \Theta_A^2$$

where Θ_A is the antenna HPBW. Calculating the integral equation (10) with the main beam equation (12a) and the source distribution equations (9a) and (9b) one obtains

Gaussian distribution with HPW Θ_s

$$(13a) \quad \begin{aligned} \Omega_s &= 1.133 \Theta_s^2 \\ \Omega_s' &= \frac{1.133 \Theta_s^2}{1 + \Theta_s^2 / \Theta_A^2} \end{aligned}$$

Disk distribution with diameter $2R$

$$(13b) \quad \Omega_s' = 1.133 \Theta_A^2 \left[1 - \exp \left\{ -\frac{R^2}{(0.6 \Theta_A)^2} \right\} \right]$$

The correction functions $\Omega_m \Omega_s / \Omega_s'$ which must be applied to calculate the flux density of an extended gaussian or disk source are drawn in figure 4a as a function of $2R/\Theta_A$ and Θ_s/Θ_A , respectively. These curves show that even for small source diameters the correction value depends strongly on the assumed source model. The rigorous calculation may be found in [33].

It can be easily shown that for a radio source with finite apparent diameter Θ_s the antenna temperature tends to a constant value, if the radio source is already resolved and the diameter D of the antenna is still increased

$$T_A(D \rightarrow \infty) = \frac{S_\nu}{2k} A \left(\frac{\Theta_A}{\Theta_s} \right)^2$$

This result leads to the following consequences which are of practical importance

- a. The antenna temperature of a resolved source with a spectral index x ($S_\nu \sim \nu^{-x}$) decreases proportionally to $T_A \sim \nu^{-(2+x)}$ since $\Theta_A \sim \lambda/D$.
- b. Compare a perfect reflector with a negligible surface deviation and diameter D_1 with a reflector with a noticeable surface deviation which consequently reduces the antenna efficiency. The diameter D_2 of the latter reflector shall be larger than D_1 by an amount which just compensates for the reduced antenna efficiency of the reflector (2) so that the effective antenna areas of the two reflectors are equal. If these two antennas are pointed to the same radio source (which shall be resolved by both antennas), then the antenna with the smaller diameter D_1 and the perfect surface yields a higher antenna temperature than the larger antenna.

The second effect can be seen in figure 8, where the calculated antenna temperatures of some radio sources are plotted over the wavelength. In the overlapping region 1 to 0.8 cm the 36-foot telescope has a higher antenna temperature than the 140-foot telescope, although the effective antenna area of the latter telescope is still considerably higher, as can be seen in figure 7.

I.3. The Observation Technique

The observation technique with large antennas at very high frequencies is governed by the integration time at the receiver output. For a switched receiver with the bandwidth B and a system noise temperature T_s of the radio telescope, the lowest practically detectable antenna temperature is determined by the peak-to-peak value of the noise fluctuations. As long as quantum noise may be neglected this value is given by

$$(14) \quad T_A = 6.4 \frac{T_s}{\sqrt{\beta\tau}}$$

τ is the time constant of the low pass filter. If this low pass filter is a simple RC-network the output voltage $v_o(t)$ is related to the input voltage $v_i(t)$ by the integral equation

$$(15) \quad v_o(t) = \frac{1}{\tau} \int_{-\infty}^t \exp\left\{-\frac{t-t'}{\tau}\right\} v_i(t') dt'$$

In the case of radioastronomical observations the input voltage is given by the antenna convolution integral, equation (6), the scan speed of the radio telescope, and the detector law. A reasonable assumption for the numerical evaluation of equation (15) is a square law detector and a gaussian-shaped source distribution function with the HPW Θ_s . Then the observed scan curve is also a gaussian curve with the HPW $\Theta_A' = \Theta_s \left(1 + \frac{\Theta_s^2}{\Theta_A^2}\right)^{1/2}$. If v_s is the scan speed of the telescope, then an angular distance $\Delta\Theta$

can be converted into the corresponding time $\Delta t = \Delta\Theta / v_s$. The integral equation (15) has been evaluated for this case in an earlier report [9]. It is shown that the maximum of the output curve is decreased and delayed with respect to the input curve. Only in the case

$$(16) \quad \tau \leq 0.06 \Theta_A' / v_s$$

is the decrease of the maximum of the output curve negligible, the time and angular delay of the symmetry axis (but not the maximum) being $\Delta t = \tau$ and $\Delta\Theta = \tau v_s$, respectively.

For observations with a fixed antenna, equation (16) can be written in the form

$\tau \leq 4 \cdot 10^{-3} \cdot \frac{1}{\cos \delta} \cdot \frac{\Theta}{A \text{ sec of arc}}$ with δ the declination of the radio source. This equation has been plotted for point sources and declination angles $-60^\circ \leq \delta \leq +60^\circ$ for the three NRAO telescopes in figure 5. In many cases these time constants will be too small to give the high sensitivity required for observations at high frequencies, but a better adapted observation technique has to be found.

By integrating equation (15) we find a similar result as in the case of the antenna convolution integral

$$(17) \quad \int_{-\infty}^{+\infty} v_0(t) dt = \int_{-\infty}^{+\infty} v_i(t) dt$$

This means that if a distorted drift curve is integrated all information concerning the total flux of a radio source can be obtained but no, or only poor, information is obtained concerning the position and the distribution of the radio source. So this technique may only be applied in some special cases.

In all other cases we have to observe with a tracked antenna. It then may be convenient to switch the receiver between the feed horn and a sky horn, which is also directed to the reflector but displaced in the focal plane in radial direction. By means of this arrangement we not only measure directly the desired excess temperature of the radio source over the sky radiation but also may suppress the effect of short-time fluctuations in the sky noise to a certain degree.

This beam-switching technique is applied in the infrared region as well as in the mm- and cm-region. Conway [11] has pointed out in a recent paper that for a close spacing of sky horn and feed horn the cancellation of atmospheric fluctuation may become complete, since the far field of large antennas at cm-wavelengths lies outside the

* Apart from the evident loss of sensitivity of the radiometer there is another technical reason which limits the free choice of the time constant. In a switched receiver the time constant must be long enough to filter out the switch frequency.

atmosphere, so that the main and reference beams of the antenna subtend approximately the same parallel beam through the turbulence zones of the atmosphere. Although some work has been done to calculate the near field pattern of large antennas, nothing is known about the near field pattern of a radially defocused feed. Measurements with the NRAO 300-foot antenna have shown, however, that with a beam tilted 3.5 times the HPBW of the antenna from the main axes the coma lobe attenuation is only 13 db, which may cause considerable confusion problems. Not many experimental results are available. Straiton and Tolbert measured the correlation of atmospheric fluctuations at 70 GHz [31] and found approximately a gaussian correlation function with a HPW of about 10 feet. Low [private communication] reported a reduction of the sky fluctuations of 90 percent at $\lambda = 1$ mm using this switching technique.

Instead of a continuous scan curve, a set of individual points of the source are measured. This procedure allows the use of an integrator rather than a low-pass filter at the receiver output, which results finally in a better signal-to-noise ratio, as will be shown. For single sideband reception the RMS fluctuations at the receiver output are [10], if an integrator is used

$$(18a) \quad \Delta T = \frac{\pi}{2} \frac{T_s}{\sqrt{t_{\text{int}} B}}$$

with the bandwidth B and the integration time t_{int} . The RMS output fluctuations for the same receiver, using a low-pass filter are

$$(18b) \quad \Delta T = \frac{\pi}{2} \frac{T_s}{3^{1/2} \sqrt{\tau B}}$$

Combining the two equations we obtain the ratio $\Delta T_{\text{int}} / \Delta T_{\text{lowp}} = (2\tau/t)^{1/2}$. Since one has to wait at least four times the time constant τ to read an average value using a low-pass filter, it is evident that an integrator improves the minimum detectable antenna temperature by at least a factor $\sqrt{2}$.

* Burns [36] shows that there is a continuous transition between the two cases of an integrator and a low-pass filter.

We wish to know the largest spacing of the measuring points without losing any information concerning the structure of the radio source. This question may be answered by the sampling theorem which states that a function with the spectral bandwidth B is completely determined by its values taken at equi-distant points with a spacing of $1/2 B$. If the distribution function of the radio source is represented by its Fourier integral, it can be shown that the gaussian main beam acts as a low pass filter for the spatial frequencies. The bandwidth of this low-pass filter is $B = 1/(1.06 \Theta_A)$. Then it follows that the measurements have to be spaced half the HPBW apart.

II.2. Antennas

We consider four paraboloid antennas: (1) The NRAO 140-foot antenna, (2) the NRAO 85-foot antenna, (3) a 36-foot antenna which will be built at the NRAO, and (4) the 12-foot antenna of the NRAO. The principal characteristics of these antennas are listed in the following table.

TABLE 2

Diameter D		RMS Deviation $\sqrt{d^2}/\text{mm}$	HPBW $\Theta_A/\text{sec of arc}$	Antenna Efficiency η_0	Efficient Antenna Area A_0/m^2	Main Beam Solid Angle $\Omega_m/(\text{sec of arc})^2$
ft.	m					
140	42.7	1*	$58.6 \lambda/\text{cm}$	0.65	930	$3.9 \cdot 10^3 \left(\frac{\lambda}{\text{cm}}\right)^2$
85	26	3.2**	$96 \lambda/\text{cm}$	0.60	318	$1.04 \cdot 10^4 \left(\frac{\lambda}{\text{cm}}\right)^2$
36	11	0.06***	$22.8 \lambda/\text{mm}$	0.55	52	$589 \left(\frac{\lambda}{\text{mm}}\right)^2$
12	3.66	0.04^{***} $1/$	$68.4 \lambda/\text{mm}$	0.50	5.3	$5.3 \cdot 10^3 \left(\frac{\lambda}{\text{mm}}\right)^2$

* Expected value.

** Measured values (reference [12]).

*** Scheduled value.

1/ Preliminary measurements of the 12-foot surface indicate the scheduled values to be optimistic.

The HPBW of the antennas have been calculated from the semi-empirical formula.

$$(19) \quad \frac{\Theta_A}{\text{sec of arc}} = 2.5 \cdot 10^5 \frac{\lambda}{D}.$$

Θ_A has been plotted for the four antennas as a function of wavelength in figure 6. The main beam solid angle

$$(20) \quad \frac{\Omega_m}{[\text{sec of arc}]^2} = 1.133 \Theta_A^2 = 7.1 \cdot 10^{10} \left(\frac{\lambda}{D}\right)^2$$

can be calculated.

The antenna efficiencies η_o of the undisturbed (ideal) reflectors have been estimated, taking into account the fact that the aperture blocking effect decreases generally with increasing aperture diameter. It should be reminded that the effective antenna area $A = A_g \cdot \eta_A$ includes already the losses of the feed and the reflector. Therefore, the well-known relation between effective area and antenna gain G takes the form

$$(21) \quad \frac{A}{\lambda^2} = \frac{\eta_R}{\Omega} = \frac{\eta_R(1 - \beta_m)}{\Omega_m} = \frac{\eta_B}{\Omega_m}$$

$$\eta_B = \eta_R (1 - \beta_m) \text{ is the beam efficiency.}$$

Here the antenna gain is expressed by the antenna solid angle Ω and the main beam solid angle Ω_m , main beam stray factor β_m , and beam efficiency η_B , respectively. For a well-designed antenna the shortest wavelength, at which the radioastronomical observations can be made, is determined by the RMS deviation of the reflector from its designed parabolic form. We refer to the literature for a detailed discussion [12], [13]. The effective area of an antenna with the RMS deviation $\sqrt{d^2}$ at a wavelength λ is given by Ruze's formula

$$(22) \quad A(\lambda) = A_o \exp \{-16\pi^2 \overline{d^2}/\lambda^2\}$$

This equation has been evaluated with the values A_o and $\overline{d^2}$ for the antennas taken from table 2. The results are shown in figure 7.

Theoretical investigations show — and experimental results confirm — that even in the case when the antenna efficiency has been reduced by a factor 5 due to the random deviations of the reflector the HPBW (and therefore the main beam solid angle) obey the equations (19) and (20), respectively. If the main beam stray factor of the undisturbed reflector is β_0 , then it follows from equations (21) and (22) that the beam efficiency as a function of the wavelength is $\eta_B(\lambda) = \eta_{B_0} \exp\{-16\pi^2 \bar{d}^2/\lambda^2\}$. With increasing ratio \bar{d}^2/λ^2 more and more of the power which is captured by the reflector is diffusely reflected causing an exponential increase of the stray region solid angle Ω_{stray}

$$\Omega_{\text{stray}} = \int_{\text{stray}} f d\Omega$$

The physical interpretation of this effect is that, since power is subtracted from the main lobe, the on-axis gain of the antenna decreases and consequently the relative sidelobe level with respect to the main lobe also decreases. This decrease in sidelobe attenuation limits the useful range of an antenna at high frequencies rather than the decrease in gain and effective area. As may easily be shown the antenna gain as a function of wavelength reaches its maximum value at the wavelength $\lambda = 4\pi\sqrt{\bar{d}^2}$ where the effective area of the antenna has dropped to $e^{-1} = 0.37$ times the value of the undisturbed reflector.* The effect of the random deviations of the reflector have been discussed in detail by Ruze [13]. Conforming to his theory the decrease in attenuation of the first sidelobes due to a RMS deviation $\sqrt{\bar{d}^2}$ and a correlation interval C of the random deviations is

$$(23a) \quad f(r) = f_0(r) + \frac{4}{\eta_A} \left[\frac{4\pi C d}{D\lambda} \right]^2 \exp\left\{-\left(\frac{\pi r C}{\lambda}\right)^2\right\}$$

* $\lambda = 4\pi\sqrt{\bar{d}^2}$. At this wavelength also occurs the maximum antenna temperature of a planet, whose diameter is smaller than the HPBW of the antenna, as may be seen in section III.3.

Here r is the angular distance from the antenna main axes, $f_0(r)$ is the antenna power pattern in absence of errors and the second term is the increase in the sidelobe level due to the errors. The aperture efficiency η_A decreases with increasing ratio d/λ . At $\lambda = 4\pi d$ where the antenna gain as a function of wavelength reaches its maximum value and which is normally considered to be the shortest wavelength for observations with a particular antenna $\eta_A(\lambda) = 0.37 \eta_A$ of the undisturbed reflector. If we express the sidelobe level due to the surface irregularities in the immediate neighborhood of the main beam in db, we find

$$(23b) \quad 10 \log \left[\frac{\eta_A}{4} \left(\frac{D}{C} \right)^2 \right]$$

To obtain a sidelobe attenuation of at least 10 db, one finds that the correlation interval C of the antenna must be $C \leq 0.061 D$. This condition is normally fulfilled with a well designed reflector; it shows, however, that a large-scale deflection of the reflector can be very dangerous for the ultimate performance of the antenna at very short wavelength.

To estimate the influence of the sidelobes on radioastronomical observations we use the following, very simplified, model of the antenna pattern.

$$f(r) = \sum_i a_i \exp \left\{ - \frac{(r - r_i)^2}{(0.6 \Theta_i)^2} \right\}$$

Here r is the angular distance from the antenna axis, r_i is the distance where the maximum of the i^{th} sidelobe occurs and Θ_i is the HPW of the i^{th} sidelobe ($\Theta_1 = \Theta_A$) ($r_1 = 0$).

To calculate the antenna solid angle we integrate the pattern

$$\begin{aligned} \Omega &= 2\pi \int_0^\infty dr r f(r) = \pi(0.6 \Theta_1)^2 + 2\pi^3 \sum_{i \leq 2} a_i r_i (0.6 \Theta_i) \\ &= \Omega_m \left[1 + 5.9 \sum_{i \leq 2} a_i \frac{r_i \Theta_i}{\Theta_A^2} \right] \end{aligned}$$

These equations hold for $r_i/0.6 \Theta_i \gg 1$. Now $\Omega_m = \pi(0.6 \Theta_A)^2$ is the main beam solid angle and so it is convenient to normalize the contribution of the sidelobes with respect to the antenna solid angle.

Since we are only concerned with the first sidelobes we can make the following assumptions: $\Theta_i = 0.3 \Theta_A$ and $r_2 = 1.7 \Theta_A$; $r_i = 1.7 \Theta_A + 0.8 (i - 2) \Theta_A$ and we obtain the result

$$(24) \quad \Omega = \Omega_m \left\{ 1 + 1.4 \sum_{i \geq 2} a_i [2.1 + (i - 2)] \right\}$$

$$= \Omega_m [1 + 2.9a_2 + 4.3a_3 + \dots]$$

If the antenna is pointed to an uniformly bright source, the ring-shaped zone between the first and the second minimum of the diffraction pattern collects $2.9a_2$ times the radiation power collected by the main beam. With an average attenuation of the first sidelobe of 10 db ($a_2 = 10^{-1}$), this is about 30 percent of the radiation power which is collected in the main beam, and one may have considerable confusion problems if an extended source is observed.

There are some arguments as to whether radomes shall be used to protect the high-precision telescopes used in mm-wave radioastronomy. Several radioastronomers are inclined to believe that the advantages of a telescope housed in a radome and operated at a constant ambient temperature will compensate the slight decrease in system sensitivity, as long as the total absorption of the radome does not exceed 1 db. It should be possible, however, to remove the radome without too much complication to allow for absolute measurements. Anway [14] has indicated that the radome can act as a random refracting screen, which implies a possible limitation of the radome's utility.

The focusing as well as the calibration of antennas at very high frequencies may cause difficulties. The only available strong radio sources are the sun, the moon, and the planets. It will be difficult to focus the feed of an antenna using a source like the sun or moon, whose diameter is considerably larger than the HPBW of the antenna.

P. Stumpff [20] investigates the possibility of using drift curves of the moon for the determination of the antenna HPBW. The curves in figure 4b are taken from his numerical calculations. They represent the convolution of a gaussian main beam (equation 12a) with the disk distribution (equation 9a). Parameter of the curves is the ratio of the source diameter $2R$ to the HPBW Θ_A of the antenna. For $2R/\Theta_A = 1$, the form of the convolution curve deviates only little from a gaussian curve. The HPBW r_{hp} of the observed drift curve is then approximately related to Θ_A and $2R$

$$(25) \quad (2r_{hp})^2 = \Theta_A^2 + \frac{\ln 2}{2} (2R)^2 \quad \sqrt{\frac{\ln 2}{2}} = 0.5888$$

With decreasing the HPBW of the antenna the HPW of the observed drift curve gets smaller and smaller and reaches a minimum value at $2R = 2.3 \Theta_A$. With further decreasing the HPBW of the antenna the HPW of the drift curves approaches finally the value $2r_{hp} = 2R$. For $2R/\Theta_A \geq 10$ the convolution of the gaussian main beam with the disk can be treated as a convolution with an infinitely extended plane. This result will be of importance for observations in the cm- and mm-region, where the strongest sources have approximately disk distributions.

II. 2. Receiver

Two different types of radiometer systems are used for observations at very high frequencies:

1. The coherent detection system, which maintains the phase information of the detected radiation. This comprises superheterodyne receivers, masers, and parametric amplifiers, tunnel diode amplifiers, and traveling wave tubes.
2. The direct or power detecting systems (sometimes also called quantum counters) which convert the high frequency radiation directly in DC. Crystal rectifiers, barretters, bolometers, and Golay cells represent this type of detectors.

The coherent detectors have the advantage, that their bandwidth is determined by the amplifiers itself, that they have relatively low noise temperatures and that all phase information is available. Their disadvantages are: High costs and very sophisticated electrical systems as well as relatively small bandwidths.

The direct or power detectors have the advantage that their electronic systems are generally very simple as compared to the coherent detectors, resulting in lower prices and higher reliability. Also, most of these detectors are sensitive over a very large bandwidth. But often this advantage turns out to be also a disadvantage of direct detectors, since input filters must be used to shield the detectors of unwanted radiation. Also, as will be shown, the sensitivity of most direct or power detectors when related to the same bandwidth is poor as compared with the available coherent detectors.

To compare the performance of the two kinds of radiation detectors we follow the analysis of Long and Rivers [15]. The minimum power which can be detected with a given power detector is (Minimum Detectable Power = MDP)

$$(26) \quad \Delta P = K\sqrt{B_V}$$

K is called the sensitivity of the detector, which is defined as the minimum detectable change in radiation power referred to a 1 Hz video bandwidth. The MDP decreases with the square root of the video bandwidth B_V .

The RMS fluctuations at the output of a coherent detecting radiometer are described as the RMS voltage fluctuations, expressed in °K change of the antenna temperature. For a switched receiver is $\Delta T_R = \pi T_S / 2^{3/2} (B_R \tau)^{1/2}$ with a bandwidth B_R , the time constant τ of the low pass filter and the system noise temperature T_S . The MDP can be expressed as antenna temperature change using the Rayleigh-Jeans approximation. Then $\Delta T_D = \Delta P / 2k B_D$ where $k = 1.38 \cdot 10^{-23}$ Ws/°K and B_D is the useful bandwidth of the detector.* "Useful bandwidth" means that either the bandwidth is determined by

* The factor 2 must be used here since a bolometer — in contradiction to any coherent detector — accepts all directions of polarization.

the receiver itself or by the atmosphere. Equating $\Delta T_D = \Delta T_R$ we obtain a relation between the detector sensitivity K and the system noise temperature T_s of the coherent radiometer

$$(27) \quad \frac{T_s}{\sqrt{B_R}} = 2.31 \cdot 10^{22} \frac{K}{B_D}$$

Here the relation $\tau = 1/2B_V$ has been used. Assuming now that the bandwidth of the power detectors are larger than the bandwidth of the windows in the atmosphere, we can insert in equation (27) the values B given in table 1 in order to compare the available coherent and power detectors.

We will give here only a very short review of some characteristics and achieved performances of coherent detectors. In appendix II Mr. E. W. Kinaman of the Watkins Johnson Corporation gives a review on the present state and the future development of traveling wave tubes (TWT). The TWT's are of special interest for work at very high frequencies because they do not need a pump source and since they have broadband characteristics comparable to that of non-coherent detectors.

In figure 14 the noise temperatures of various types of low-noise pre-amplifiers are given for signal frequencies up to 20 GHz. These curves have been prepared by M. Lebenbaum of Airborne Instruments Laboratory.

A. Superheterodyne receivers. The performance of mixing detectors starts falling off when the shunt effect of the junction capacitance becomes considerable. The higher the conductance of the junction the shorter the wavelength λ at which the conversion loss increases very rapidly. One obtains the selection of semiconductor materials, usable as mixing elements: Si ($\lambda = 3$ cm), Ge ($\lambda = 5$ mm), GaAs ($\lambda = 1$ mm). InSb should be superior to these three materials but experimental results have been disappointing according to Putley [29]. A report on the performance of superheterodyne receivers using GaAs junctions which are mounted without case in a waveguide is given in [16]. The values in table 3 for the noise temperature and bandwidth of superheterodyne receivers have been partly taken from this paper. It should be considered, however, that harmonic mixing has been used at the higher frequencies, which may increase the noise temperature considerably. The highest frequency for which superheterodyne receivers have been built (apart from optical mixers) is 600 GHz ($\lambda = 0.5$ mm) as far as we know.

B. Parametric amplifiers. Parametric amplifiers are now commercially available up to 35 GHz. Cooled parametric amplifiers using either InSb varactor diodes cooled to 77 °K or GaAs diodes cooled to 4 °K may compete with the noise temperatures of masers in the cm wave region. As far as the bandwidth is concerned, paramps are superior by a factor 10 to 100. A review of the state of technique of parametric amplifiers is given in figure 14. Parametric amplifiers for the 100 GHz region may be available within the next year, with noise temperatures of around one hundred degrees K and a bandwidth of about 1 GHz.

C. Maser. The practical use of masers in the cm-wave region has become doubtful because of the progress in the development of low-noise parametric amplifiers. Traveling wave masers have the advantage of not needing a circulator or isolator; also, the gain of a maser becomes independent on the pump power above a certain saturation level. The highest frequency at which a maser has been worked until now is 70 GHz [30].

D. Tunnel diode amplifiers. A review on the commercially available tunnel diode amplifiers, based on the production program of the Micro State Electronics Corporation is given in appendix I. With the diodes available today the frequency range of these amplifiers is limited to about 16 GHz. The frequency range may be extended to higher frequencies by using diodes which are mounted without case in a waveguide. The noise temperature of the tunnel diode lies between that of crystal mixers and paramps or masers. Considering the bandwidth, tunnel diode amplifiers are superior to masers and paramps but not to TWT's. The noise temperature of tunnel diode amplifiers may be considerably improved by using cooled InSb diodes. The use of tunnel diode amplifiers as IF amplifiers for superheterodyne receivers in the mm- and sub-mm wave range will be limited to the first stages because of the low saturation level (about -25 dbm output power).

E. Traveling wave tubes. Because of their very large bandwidth TWT radiometers have been widely used in the past years at 3 and 8 GHz, but their importance has decreased after relatively inexpensive and reliable low-noise preamplifiers have become available in the cm region. Recently the development of a broad-band low-noise TWT for the 3 mm region has been reported [17]. The state of technique as well as the development

which may be expected within the next two years is reviewed in appendix II. A big advantage of TWT's is that they do not need a high frequency pump source. On the other hand, their very broadband amplification involves some problems as far as switches and detectors are concerned.

In table 3 we give some examples of radiometers for the mm-wave region with their corresponding values for the system noise temperatures and bandwidths. Most of these receivers have been quoted in the recent literature. So it may be concluded that at present coherent detectors with lower noise temperature and broader bandwidth are in operation, at least in the laboratories. The values $T_S/\sqrt{B_R}$ given in this table represent also the RMS noise fluctuations, if these receivers are used as total power receivers with a time constant of $\tau = 1$ sec. In the last column the sensitivity K of that power detector is indicated, which would have the same temperature resolution as the corresponding coherent radio receiver when operated with an input bandwidth B_D . These values K vary between 10^{-14} and 10^{-11} W · (Hz)^{-1/2}.

To compare now the sensitivity of coherent detectors with available power detectors, we give in table 4 some values of existent power detectors. These values are based on a review given by Putley [29]. Crystal-video detectors which are also used in the mm-wave region have been reported to have sensitivities down to $5 \cdot 10^{-12}$ [15]. Low (private communication) claims a sensitivity of his He-cooled bolometer between $3 \cdot 10^{-14}$. With the exception of Low's bolometer the sensitivity of most of the coherent detectors is better than the sensitivity of power detectors. One should bear in mind, however, that most of the power detectors mentioned in table 4 work also in the sub-mm and infrared region where — with the exception of one superheterodyne receiver for $\lambda = 0.5$ mm — no coherent detectors exist at present.

From this comparison it can be concluded that even with the present state of technique coherent detectors can compete with the most sensitive bolometers up to the 3-mm band. For higher frequencies the bolometers are superior in sensitivity as well as the radiometers are superior for lower frequencies. In the case of narrow-band detection (observation of lines) as well as in the case of interferometry, however, the advantages of coherent detectors are obvious even at frequencies higher than 100 GHz.

TABLE 3

Band	Type of amplifier	Manufacturer	Reference	Band-width B_R /GHz	System noise temperature T_s /°K	$\frac{T_s}{\sqrt{B_R}}$ /°K · Hz ^{-1/2}	$\frac{B_D}{\text{GHz}}$	Equivalent sensitivity K/W · Hz ^{-1/2}
8.6 mm	Superheterodyne	Ewen-Knight	[19]	0.012	$1.5 \cdot 10^3$ (s. c.)	0.43	16	$3 \cdot 10^{-13}$
	TWT	Watkins-Johnson	*	16	$3.8 \cdot 10^3$	$3 \cdot 10^{-2}$	16	$2.1 \cdot 10^{-14}$
	Maser	AIL	[18]	0.075	$1.3 \cdot 10^2$	$1.5 \cdot 10^{-2}$	16	$1 \cdot 10^{-14}$
3.5 mm	Superheterodyne	ECI	*	1	$5 \cdot 10^3$ (d. c.)	$1.5 \cdot 10^{-1}$	30	$2.0 \cdot 10^{-13}$
	TWT	Watkins-Johnson	[17]	28	$9 \cdot 10^3$	$5.4 \cdot 10^{-2}$	30	$7.0 \cdot 10^{-14}$
2.0 mm	Superheterodyne	ECI	[16]	1.5	$3 \cdot 10^4$ (d. c.)	$7.8 \cdot 10^{-1}$	35	$1.2 \cdot 10^{-12}$
1.2 mm	Superheterodyne	ECI	[16]	1.5	$1.2 \cdot 10^4$ (d. c.)	3.1	90	$1.2 \cdot 10^{-11}$

* Private communication.

s. c. — single channel noise temperature.

d. c. — double channel noise temperature.

TABLE 4 (taken from Putley [29])

Detector	Sensitive area mm ²	Operating temperature °K	NEP for 1 cps bandwidth w (= sensitivity K)	Responsivity vpw	Response time sec.	Operating wavelength and other conditions
Golay pneumatic detector	1.5	300	$3 \cdot 10^{-10}$	$\sim 10^5$	0.015	$\lambda < 5$ mm
Carbon bolometer	20	2.1	$1 \cdot 10^{-11}$	$2.1 \cdot 10^4$	0.010	Operates over whole of sub-mm band at least.
Germanium bolometer	{ 15 15	2.15 2.15	$5 \cdot 10^{-13}$ $3 \cdot 10^{-12}$	$4.5 \cdot 10^3$	$4 \cdot 10^{-4}$	} As for carbon bolometer.
Superconducting tin bolometer	{ 6	3.7	$3 \cdot 10^{-12}$	—	1.25	As for carbon bolometer.
Ideal photoconductive detector	{ 100 100 100	1.5 1.5 1.5	$6.5 \cdot 10^{-13}$ $6.5 \cdot 10^{-14}$ $1.8 \cdot 10^{-14}$			{ $\lambda = 100 \mu$. 300°K background for $\lambda > 100 \mu$. $\lambda = 1000 \mu$. 300°K background for 10 per-cent band at 500μ .
InSb wide-band detector using magnetic field	{ 5	1.5	$2 \cdot 10^{-11}$ $1 \cdot 10^{-11}$ $5 \cdot 10^{-12}$	{ 200 500 1000	$2 \cdot 10^{-7}$	{ $\lambda = 200 \mu$ $\lambda = 500 \mu$ $\lambda = 1000 \mu$
InSb detector without magnetic field	15	4	10^{-12}		$3 \cdot 10^{-7}$	{ λ 0.5 to 8 mm. This sensitivity was achieved with a narrowband amplifier not permitting full exploitation of fast response.
Ge cyclotron resonance detector	2	4	$2 \cdot 10^{-12}$	10^6	$5 \cdot 10^{-9}$	$\lambda = 8$ mm
Tuned InSb detector	25	4	$5 \cdot 10^{-11}$		10^{-6}	{ Responds over a bandwidth of about 12 percent within range $150 \mu - 60 \mu$.
Meredith and Warner video receiver	{ —	300 300	$2.5 \cdot 10^{-11}$ $4 \cdot 10^{-9}$	— —	10^{-9} 10^{-9}	$\lambda = 2$ mm $\lambda = 1$ mm

III. Observations

We divide this section in three paragraphs concerning the observations of extragalactic sources, of H_{II} regions and of the planets and the moon. The aim of this report is not to stimulate any specific radioastronomical observing program, but rather to show what can be observed with a given antenna considering the limitations due to either the instruments or the atmosphere. The results may then be used to determine the most favorable observing frequencies.

Until now we have only considered the atmosphere as a source of interference. Even if man-made noise at frequencies $\nu \geq 3$ GHz is not considered to be such a severe problem that it is for observations at lower frequencies, it should be considered as a possible source of interference. The frequency bands for observations should be selected, if it is possible, as to fit the bands which are protected for radioastronomical observations. These bands are for wavelengths $\lambda \leq 11$ cm listed in the following table.

TABLE 5

ν /GHz	λ_0 /cm	B/MHz
2.690 - 2.700	11.1	10
4.990 - 5.000	6.0	10
10.680 - 10.700	2.8	20
15.350 - 15.400	1.95	50
19.300 - 19.400	1.55	100
31.300 - 31.500	0.955	200
Above 40.000	No allocations made up to now.	

Before we start with the consideration of different types of radio sources — thermal and non-thermal — we will calculate the antenna temperature of three of the strongest radio sources: Cas A with a typical non-thermal spectrum ($S \sim \nu^{-0.8}$), Tau A with an extremely flat spectrum ($S \sim \nu^{-0.25}$) and Orion with a typical thermal

spectrum ($S \sim \nu^{-0.1}$). The apparent diameters of all three sources are about 4' [22]. Using then equations (9) and (10) and the effective antenna areas from figure 7, we can calculate the antenna temperatures which could be expected in the four NRAO antennas at different wavelengths. The results are shown in figure 8. Since the absolute spectra of these radio sources are only known for $\lambda \geq 3$ cm we have extrapolated this spectra to shorter wavelengths.

The general feature is that the antenna temperatures of all radio sources decrease very rapidly with wavelength. This is not only due to the spectral behavior of these sources but also to the finite angular extension. The factor Ω_s'/Ω in equation (9) becomes for $\Theta_A = 68''$ (36-foot telescope at $\lambda = 3$ mm) and $\Theta_s = 240''$ $\Omega_s' = \Omega = 13.4$. If it would be possible to collect in the feed the whole radiation power incident on the aperture of the antenna, the antenna temperatures of the three radio sources would range between 1.9 and 8 °K. As we will see in paragraph 3 the situation becomes much worse in the case of the emission nebulae.

By only extrapolating the microwave spectrum of the known radio sources it seems to be very doubtful if observations at 3 mm wavelength or shorter can contribute anything to the radioastronomy of galactic and extragalactic sources. On the other hand there is some evidence of radio sources of very small apparent diameters with flat or even increasing spectra which may become well "visible" at very short wavelengths. Apart from a few emission nebulae with very high emission measures there is little hope to observe the continuous radiation of ionized hydrogen clouds. It might be possible, however, to observe a line radiation of H_{II} clouds, as will be discussed in more detail in paragraph 2.

There is no argument about the value of observations of the planets and the moon in the mm-wave region, and as will be shown in paragraph 3 of this section the antenna temperatures which can be expected with the NRAO antennas will allow detailed investigations of the planetary radiation.

III. 1. Extragalactic Radio Sources

To evaluate the number of extragalactic radio sources observable with a given antenna at the wavelength λ , we use a statistical approach introduced by von Hoerner [23] with only two slight changes:

- a. It can be expected with the present state of technique, as we have shown in paragraph II. 2, that the minimum detectable change in the antenna temperature is limited by the sky temperature fluctuations rather than by the system noise.
- b. The resolution of an extended source — described by the factor Ω_s' / Ω_s in equation (9) — must be considered.

If the RMS fluctuations of the sky temperature are denoted by ΔT_{fl} , then the minimum detectable flux density is given by

$$(28) \quad S_{\min} = \frac{2k}{A} (5\Delta T_{fl}) (1 + \Theta_s^2 / \Theta_A^2)$$

where a signal-noise ratio of 5 has been chosen as an appropriate value. Following von Hoerner we assume $S \sim \lambda^x$ ($x = 0.8$) and for the number of available sources $N_{av} \sim S^{-n}$ ($1.5 \leq n \leq 2$). Combining these equations and assuming that above 75 percent of the sky is visible at Green Bank, we get for the total number of "visible" sources the expression

$$(29) \quad N = 141.3 \left[\frac{2.18 \cdot 10^{-5}}{(1 + \Theta_s^2 / \Theta_A^2)} \frac{(\text{A/m}^2) (\lambda/\text{cm})^{0.8}}{(\Delta T_{fl} / ^\circ\text{K})} \right]^n$$

We have evaluated this equation for the 140-foot antenna, taking the effective antenna area from figure 7 and a mean value for ΔT_{fl} from figure 3. To get an estimate of the angular sizes of extragalactic radio sources we take the values given by Bolton [24]: 40(49) percent of all observed objects have an angular size of less than 0.4', 72(73) percent of all objects have an angular size of less than 1.6'. The HPBW of the 140-foot

antenna is about 2' at 2 cm wavelength. We may neglect therefore the effect of a finite source extension for a first evaluation of equation (29) although the factor $(1 + \Theta_s^2/\Theta_A^2)$ will affect the result only at short wavelengths, where the number of visible sources becomes very small. The results of the evaluation of equation (29) with two different exponents $n = 1.5$ and $n = 2$, respectively, are listed in the following table.

TABLE 6

λ/cm	A/m^2	$\Delta T_{\text{fl}}/^{\circ}\text{K}$	N_{vis}	
			$n = 1.5$	$n = 2$
10	900	0.4	771	1360
9	900	0.042	599	954
8	900	0.044	508	780
7	900	0.046	408	581
6	890	0.048	311	403
5	870	0.05	226	266
4	840	0.06	126	122
3	780	0.07	63	48
2	620	0.17	7	3

Evidently there is no sense in extending this statistical treatment to shorter wavelengths. This confirms our guess that by only extrapolating the results obtained in the lower frequency range of the radio spectrum one would hardly be encouraged to look for extragalactic objects in the mm-wave range.

III.2. H II Regions

The flux density of H II regions, which are not opaque, varies $\sim \nu^{-0.1}$, whereas the flux density of most of the non-thermal sources varies $\sim \nu^{-0.8}$. So it is obvious that H II regions will become relatively intensive radio sources in the cm- and mm-wave regions.

To calculate the radiation temperatures of H II regions between 10 cm and 1 mm wavelength we start from our survey at $\lambda = 11$ cm [26] and from measurements of the Orion nebula at 8 GHz by Menon [27]. We obtain the following information

- a. At $\lambda = 11$ cm about 46 sources which have been observed are probably emission nebulae.* Of these, 46 sources have
 - 19 diameters $> 10'$
 - 14 diameters $5'$ to $10'$
 - 13 diameters $< 5'$
- b. The highest known emission measure of about 10^7 has been observed in the nucleus of Orion [27]. Between 10 and 20 emission nebulae may be expected to have emission measures $> 10^5$.
- c. Apart from very limited regions the electron density does not exceed 10^2 cm^{-3} .
- d. The excitation temperatures of the H II regions range between 6 and 12×10^3 °K.
- e. The optical depth of ionized hydrogen may be represented with sufficient accuracy in the wavelength region $10 \text{ cm} \geq \lambda \geq 1 \text{ mm}$ by the formula

* This number may turn out to be too high if more measurements with sensitive receivers at wavelengths shorter than 10 cm are available. It might then be found that some of the galactic sources have flat spectra down to about 10 cm wavelength but that their spectrum decreases more rapidly at shorter wavelength.

$$(29) \quad \tau = 1.645 \cdot 10^5 \left(\frac{T_e}{^\circ\text{K}} \right)^{-1.35} \left(\frac{\nu}{\text{MHz}} \right)^{-2.1} \frac{E}{\text{cm}^{-6} \text{ pc}}$$

which becomes

$$(30) \quad \tau = 0.655 \left(\frac{\nu}{\text{MHz}} \right)^{-2.1} \frac{E}{\text{cm}^{-6} \text{ pc}} \quad \text{for } T_e = 10^4 \text{ } ^\circ\text{K}$$

At $\lambda = 10$ cm and with $E = 10^7$ we get $\tau = 0.4$. We can calculate therefore the radiation temperature of the ionized hydrogen using the approximation $T_b = \tau T_e$. This temperature has been plotted for $T_e = 10^4$ and emission measures $10^7 \geq E \geq 10^3$ in figure 9. It is known from observations of Orion [27] as well as from recent measurements with 4.4 min of arc pencil beam antenna at $\lambda = 10$ cm [33] that regions with high emission measures have very small apparent diameters and the high angular resolution of large antennas in the cm- and mm-wave region may therefore lead to higher antenna temperatures than would be expected by extrapolating the measurements at 11 cm, which are average values over a solid angle of about 10 min of arc.

With the 140-foot telescope at $\lambda = 3$ cm it should be possible to detect most of the emission nebulae with $E \geq 5 \cdot 10^3$. This means we should be able to observe all H II regions which we have observed at $\lambda = 11$ cm with a 25-m telescope. It also should be possible to observe the thermal radiation of various galaxies.

At $\lambda = 3$ mm it will become hard to detect nebulae with $E < 10^6$. The chance to observe any extragalactic thermal radiation seems to be extremely small.

Besides the free-free transitions (deflections of an electron in the coulomb field of a proton) there exists also free-bound transitions (the electron is captured by the nucleus). After the recombination the captured electrons populate the upper levels of the hydrogen atoms falling stepwise down from the orbit with the quantum number n to the orbit with the quantum number $(n - 1)$ (cascade transitions) emitting a radiation of the frequency

$$(31) \quad \frac{\nu}{\text{Hz}} = 3.288057 \cdot 10^{15} \left[\frac{1}{(n-1)^2} - \frac{1}{n^2} \right]$$

The possibility of an observation of such a line radiation in the radio frequency range has been pointed out by Kardaschew [28] in 1959. He showed that for electron densities $n \leq 10^3$ the level with the quantum number $n = 500$ will still be populated and that the transitions $n \rightarrow (n - 1)$ have the highest probability. By considering the various line-broadening effects he came to the conclusion that for $\nu > 7$ GHz the Doppler-broadening will become the most important effect. He obtained for the line-width

$$(32) \quad B = 4.3 \cdot 10^{-7} \cdot T_e^{1/2} \nu$$

and for the radiation temperature in the line-center

$$(33) \quad T_L = 2.33 \cdot 10^{12} \frac{E}{T_e^{2\nu}}$$

Using now equation (29) for the optical depth of ionized hydrogen rather than the approximation used by Kardaschew we obtain for the ratio of line temperature to the radiation temperature of the continuous radiation

$$(34) \quad T_L/T_K = 3.56 \cdot 10^{-6} \frac{\nu^{1.1}}{T_e^{1.65}}$$

Expressing ν in GHz and taking $T_e = 10^4$ we obtain

$$(35) \quad T_L/T_K = 5.46 \cdot 10^{-3} \left(\frac{\nu}{\text{GHz}} \right)^{1.1}$$

Using these equations the values in table 7 have been calculated. The first column gives the quantum numbers, the second column gives the corresponding frequencies, the third column gives the linewidth, and the fourth column gives the spacing of the lines. By multiplying the values T_L/T_K of the fifth column with the antenna temperature of Orion plotted in figure 8 we finally obtain the antenna temperatures of the lines in column six which we may expect to observe with the different NRAO antennas, provided that Kardaschew's assumptions are correct. It is interesting to note that there is for each antenna an optimum frequency where the antenna temperature due to line radiation becomes a maximum. For the 140-foot antenna the optimum frequency is about 10 GHz.

TABLE 7

Quantum number n	ν_L /GHz (eq. 31)	B/MHz (eq. 32)	$\nu_n - \nu_{n+1}$	T_L/T_K (eq. 35)	$\frac{T_L}{^\circ K} = \frac{T_L}{T_K} T_A$ (Orion)
29	284.251	12.22	27.95 GHz		
30	256.302	11.01	24.40 GHz	2.43	0.16 (36-foot)
31	231.901	9.97			
35	160.211	6.89	13.16 GHz		
36	147.047	6.32	11.76 GHz	1.32	0.4 (36-foot)
37	135.286	5.81			
43	85.688	3.68	5.78 GHz		
44	79.913	3.43	5.27 GHz	0.67	0.47 (36-foot)
45	74.645	3.21			
57	36.466	1.57	1.87 GHz		
58	34.596	1.49	1.64 GHz	0.26	0.91 (36-foot)
59	32.852	1.41			
85	10.900	0.469	378 MHz		
86	10.522	0.452	361 MHz	$6.9 \cdot 10^{-2}$	4.5 (140-foot)
87	10.161	0.437			
109	5.149	0.221	140 MHz		0.9 (85-foot)
110	5.009	0.215	135 MHz	$3.2 \cdot 10^{-2}$	2.9 (140-foot)
111	4.874	0.209			

III.3. Planets and Moon

In two papers given at the IV URSI General Assembly in Tokyo (1963) the radio-astronomical observations of the moon and the planets made up to now (Haddock [25]) and scheduled at the mm- and infrared-region in the future (Weaver and Silver [8]) are reviewed. Roberts [35] also gives a review of the radioastronomical observations of the planets. So we will limit ourselves to the calculation of the antenna temperatures of the planets and the moon in the four NRAO antennas. The results of this calculation may serve as a base for the planning of more sophisticated observing program.

In the following table the apparent minimum and maximum diameter of the moon and the planets are listed together with the radiation temperatures. Apart from the well known mean value of the moon's radiation temperature, the temperature values listed in this table are taken from Weaver's calculations of the mean surface temperature of a rotating planet without atmosphere. Although it is well known that the radiation temperatures of the planets observed at cm-wavelengths are considerably higher, for the surface temperatures thus calculated, we take the latter values for the following computations in order to obtain a lower limit for the expected antenna temperatures, especially in the mm-wave range.

TABLE 8

Radio source	Apparent minimum R_{\min}	Diameter maximum R_{\max}	Radiation temperature $= T_{\text{rot}}$ from [8]	Some experimental results
Moon	14.8'	16.8'		230 °K $\lambda \geq 10$ cm
Mercury	4.8"	10.0"	471 °K	$T_{\max} = 1200$ °K (illuminated part) at $\lambda = 3.75$ cm.
Venus	9.8"	60.7"	230 °K	350 °K ($\lambda = 4$ mm) to 590 °K ($\lambda = 10$ cm).
Mars	3.9"	17.9"	219 °K	218 °K ($\lambda = 3$ cm).
Jupiter	31.7"	46.9"	88 °K	130 °K at mm and IR; + non- thermal radiation at longer wavelengths.
Saturn	15.8"	19.5"	64 °K	106 °K ($\lambda = 3.45$ cm) — 213 °K to 141 °K depending on polari- zation at $\lambda = 9.6$ cm.
Uranus	3.3"	3.6"	33 °K	
Neptune	2.0"	2.1"	32 °K	
Pluto	0.2"	0.2"	43 °K	

To calculate from these data the antenna temperature as a function of wavelength and aperture diameter we combine equations (5) and (7) and obtain

$$(36) \quad T_A = \frac{1 - \beta_m}{\Omega_m} \frac{h\nu}{k} \frac{1}{e^{h\nu/kT_s} - 1} \Omega_s'$$

With $h\nu/kT_s \ll 1$ and the expression (11) for Ω_s' of a uniformly radiating disk with radius R this equation becomes $T_A = (1 - \beta_m) T_s [1 - \exp\{-R^2/(0.6 \Theta_A)^2\}]$. The HPBW Θ_A of an antenna as well as the stray factor β_m are functions of the wavelength as may be seen from equations (19) and (22). Inserting these expressions one obtains finally

$$(37) \quad T_A = (1 - \beta_m) T_s \exp\left\{-\frac{16\pi^2 d^2}{\lambda^2}\right\} \left[1 - \exp\left\{-\frac{R^2 D^2}{(1.5 \cdot 10^5) \lambda^2}\right\}\right]$$

D is the aperture diameter, d the RMS deviation of the reflector. Using this equation and the values of R, T_s and D, d as given in tables 8 and 2 and assuming an antenna stray factor $\beta_m = 0.30$, we have calculated the antenna temperatures for the planets and the moon as a function of wavelength. The results of these calculations are shown as diagrams. Figures 10 and 11 show the results obtained for the 140-foot and the 36-foot antennas. The curves for the planets are the upper and lower limits of the antenna temperature due to the variations of the apparent diameters. In the case of the moon only average values of the antenna temperature with $T_s = 230$ °K and $R = 16'$ have been calculated.

The corresponding curves for the 85-foot and the 12-foot antennas are shown in figure 12, and only the maximum temperatures for the planets have been calculated.

Since Ω_s' increases and $1 - \beta(\lambda)$ decreases with decreasing wavelength, the curves show a well-determined maximum. This maximum occurs at a wavelength

$$(38) \quad \lambda_{opt} = \frac{RD}{1.5 \cdot 10^5} \left[\ln \left\{ 1 + \left(\frac{RD}{6\pi \cdot 10^5 d} \right)^2 \right\} \right]^{1/2}$$

R has to be inserted in sec of arc. For small values of R one obtains for this optimum

wavelength

$$(39) \quad \lambda_{\text{opt}} = 4\pi d \quad R \ll 6\pi 10^5 \cdot D d$$

which is the same wavelength at which the antenna reaches its maximum gain (section II. 1).

Some of the remote planets have very low temperatures and a question of interest is how much their radiation deviates from the Rayleigh-Jeans approximation. The Nyquist formula for the available noise power of a resistor at the temperature T, which is an equivalent expression for the noise power received by an antenna in an isotropic radiation field, can be written in the form

$$(40) \quad \frac{P}{\text{W/Hz}} = kT \frac{x}{e^x - 1} \quad \text{with } x = h\nu/kT$$

The factor $x/e^x - 1$ is then a measure for the deviation between Planck's law and its Rayleigh-Jeans approximation. This factor has been plotted as a function of the radiation temperature T for the center frequencies of the four atmospheric windows in the mm-wave region (figure 13). Even for a radiation temperature of 30 °K the deviation is only 20 percent at the highest frequency ($\nu = 270$ GHz).

Appendix I

This review of the state of technique of tunnel diode amplifiers is based on a private communication of Mr. R. Kolts, Micro State Electronics Corporation, Murray Hill, New Jersey, which we obtained during a visit on December 12, 1963. Values, which are written in brackets, belong to amplifiers which will be available within the next year.

A. 10% bandwidth amplifiers

Frequency range/GHz	3 to 8	8 to 12	12 to 16
Bandwidth	10%	10%	(10%)
Gain/db	17	17	(10-12)
Noise figure/db	4 (3.5)	4.7 (4.5)	(5.5)
Output power at which saturation starts	----- -25 dbm -----		

B. Broadband amplifiers

Bandwidth/GHz	2 to 4	4 to 6	6 to 8	8 to 10	10 to 12
Gain/db	10-12 (17)	18	18	15-18	15-18
Noise figure/db	5	6 (5)	6 (5)	6 (5)	7 (6)
Saturation level	----- -26 dbm -----				

C. (Very broad band amplifiers)

Bandwidth/GHz	(2 to 4)	(4 to 8)	(8 to 12)
Gain/db		(17-18)	
Noise figure/db	(4.5)	(5)	(5)

To extend the range of tunnel diode amplifiers above 16 GHz the technique has to be changed. An experimental tunnel diode amplifier has worked at 90 GHz, where the diode has been placed without package in the waveguide.

Appendix II. Traveling Wave Tubes

We have asked Mr. E. W. Kinaman of the Watkins-Johnson Company, Palo Alto, California, to give a short review of the present state of technique of TWT's and the development which may be expected within the next two years. We cite in the following Mr. Kinaman's letter of November 23, 1963 in which he answered our questions:

" I have compiled information on existing Watkins-Johnson tubes which are at the very least equivalent at every frequency to the best available elsewhere.

"Our standard-line tubes have octave bandwidth coverage. Above X-band the frequency coverage corresponds to standard waveguide bandwidths. Figure 15 depicts the status of our standard line, my predictions for the next two years and the long-range predictions of Watkins and Wade. On special order we may have wider bandwidth tubes having but slightly higher average noise figures. A TWT, providing coverage from 1 - 8 GHz has recently been developed.

"The predictions of figure 15 will be much lower when a breakthrough is made in the low-noise 'cold-cathode' emitters. A number of companies, including Watkins-Johnson, are presently working on the problem. Also, the advantage of operation at liquid nitrogen temperatures has not yet been fully exploited. An L-band tube operated in a liquid nitrogen vat has shown a minimum noise figure of 1.6 db, without any detrement to bandwidth. As a 'rule of thumb' one would expect cooling to lower noise figures between 1 db at L- and S-band increasing to about 2.5 db at E-band.

"I have included for the general background a plot (fig. 16) showing the effect of cathode temperature and the circuit loss-to-gain ratio on TWT noise figure. The noise figures shown do not include the effect of correlation (termed π) between the beam velocity and current fluctuations. Correlation can lower a 6.5 db noise figure for the L-band TWT several db. The WJ-224 millimeter-wave amplifier does not yet employ this mechanism (i. e. , $\pi = 0$), although its effect would be highly significant. The WJ-224 millimeter amplifier presently operates at a circuit loss-to-gain ratio of 1.11 and a cathode temperature of 1445°K. From figure it is noted that the corresponding room temperature minimum noise figure is 10.7 db.

"My predictions (fig. 15) are based on known or expected efforts and do not include a possible breakthrough in low-noise cold-cathode emitters. Further development effort on the WJ-224, or higher frequency scaled

versions, could improve the tube's performance significantly. Also, operation at super-conducting temperatures would allow utilization of a high 'confining-field' solenoid (10-20 kilogauss) with superior field uniformity without the problem of supplying external power. In addition, it is estimated that low-temperature operation will reduce circuit attenuation to about .05 db per guide wavelength, corresponding to a loss-to-gain ratio of .15. From figure 16 the corresponding noise figure is about 8 db (2.7 db below that for room temperature operation). The high confining field available at these temperatures would, in addition, allow incorporation of a 'low-velocity' drift region adjacent to the cathode for a further improvement of noise figure, perhaps reducing the traveling-wave noise figure to 5 db at 100 Gc and, of course, these are the values predicted for hot-cathode operation. An additional benefit would be the accompanying gain increase, at the lower circuit loss condition. For instance, the WJ-224 would experience a gain increase in the order of 10-15 db. "

Literature

- [1] Altenhoff, W., "Positionsgenauigkeit des Bonner 25-m-Teleskops, Refraktion und Extinktion bei 2.7 GHz", Veröffentlichung der Universitätssternwarte Bonn, No. 59, p. 27 (1960).
- [2] Menon, R., "Atmospheric Absorption in the Range of Wavelength Between 10 cms and 1 Micron", NRAO Internal Report (January 1964).
- [3] Drake, F. D., "The Position-Determination Program of the NRAO", Publications of the Astronomical Society of the Pacific, 72, 494 (1960).
- [4] Keen, N. J., "Electrical Path Fluctuations in the Atmosphere: A Preliminary Report on the Measurement of Differential Overground Path Fluctuations at 5.6 KMc", NRAO Electronics Division Internal Report No. 22 (1963).
- [5] Keen, N. J., NRAO Internal Report (in preparation).
- [6] Orhaug, T., "The Effect of Atmospheric Radiation in the Microwave Region", Publ. of the NRAO, Vol. 1, No. 14 (1962).
- [7] Venugopal, V. R., "Meteorological Conditions and Radioastronomical Observations at X-Band", The Atmospheric Sciences, 20, 372-375 (1963).
- [8] Weaver, H. F. and Silver, S., "Planetary Research in the Millimeter and Infrared Region of the Spectrum", paper presented at XIVth General URSI Assembly in Tokyo (1963).
- [9] Mezger, P. G., "Verzerrung radioastronomischer Beobachtungen durch Antennencharakteristik und Tiefpass", Zeitschrift fuer Instrumentenkunde, 11, 219 (1958).
- [10] Mann, P. A. and Mezger, P. G., "Das Aufloesungsvermoegen der HF-Empfangsanlage des Radioteleskops", Telefunkenzeitung, 113, 182 (1956).
- [11] Conway, R. G., "Measurement of Radiosources at Cm-Wavelength", Nature, 199, 1177 (1963).
- [12] Mezger, P. G., "Application of the Antenna Tolerance Theory to the NRAO 85-Foot and 300-Foot Telescopes," Electronics Division Internal Report No. 17 (1963).
- [13] Ruze, J., "Physical Limitations on Antennas", Technical Report 248, Research Laboratory of Electronics, MIT (October 30, 1952).

- [14] Anway, Private communication (November 1963).
- [15] Long, M. W. and Rivers, W. K., "Submillimeter Wave Radiometry", Proc. IRE, 49, 1024 (1963).
- [16] Cohn, M. F., Wentworth L. and Wiltse, J.-C., "High-Sensitivity 100- to 300-Gc Radiometer," Proc. IEEE, 51, 1227 (1963).
- [17] Kinaman, E. W. and Leaf, S. B., "A 45 Gc Bandwidth Low Noise TWT for the 3 mm Region", paper submitted at the IEEE Electron Devices Meeting, Washington, D. C. (October 1963).
- [18] Arams, A., Peyton, B., Baris, J. and Franseschini, J., "Packaged Millimeter Travelling Wave Maser for the 8-mm Band", paper presented at the mm- and sub-mm conference, Orlands, Fla. (1963).
- [19] Ewen-Knight Corporation, Internal Report: "Ewen-Knight Experience Relative to 8.5 mm Radiometric Systems with Digital Recording.
- [20] Stumpff, P., In preparation.
- [21] Cohn, M. F. and Wiltse, J. C., Private communication.
- [22] Mezger, P. G. and Stumpff, P., "The Measurement of the Diameter of Radio Sources with Pencil Beam Antennas", NRAO Electronics Division Internal Report No. 16 (August 1963).
- [23] von Hoerner, S., "Very Large Antennas for the Cosmological Problem", Publ. of the NRAO, Vol. 1, No. 2 (April 1961).
- [24] Bolton, J. G., "The Discrete Sources of Cosmic Radio Emission", Observations of the California Institute of Technology, No. 5 (1960).
- [25] Haddock, F., "Introductory Lecture: Radioastronomy of the Solar System", XIV URSI General Assembly, Tokyo (1963).
- [26] Altenhoff, W., Mezger, P. G., Wendker, H. and Westerhout G., "Die Durchmusterung der Milchstrasse und die Quellendurchmusterung bei 2.7 GHz", Veroeffentlichung der Sternwarte, Bonn, No. 59, 48 (1960).
- [27] Menon, T. K., "A Model of the Orion Nebula Derived from Radio Observations", Publ. of the NRAO, Vol. 1, No. 1 (1961).

- [28] Kardaschew, N. S., "The Possibility of the Observations of Line Radiation of Atomic Hydrogen in the Radio Region" (transl. title), *Astron. J. (USSR)*, XXXVI, 838 (1959).
- [29] Putley, E. H., "The Detection of sub-mm Radiation", *Proc. IEEE*, 51, 1412 (1963).
- [30] Hughes, W. E. and Kremenek, C. R., *Proc. IEEE*, 51, 856 (1963).
- [31] Straiton, A. W. and Tolbert, C. W., "Factors Affecting Earth-Satellite Millimeter Wavelength Communications", *IEEE Transaction on Microwave Theory and Techniques*, MTT-11, 296 (1963).
- [32] Bean, B. R. and Thayer, G. D., "Comparison of Observed Radio Refraction with Predicted Values Through the Use of Surface Weather Observations", *J. of Research, NBS*, 67D, 273 (1963).
- [33] Baars, J. and Mezger, P. G., "Investigation of Some Strong Radio Sources with Pencil Beam Antennas of Very High Angular Resolution" (in preparation).
- [34] Westphal, J. A., "New Observations of Atmospheric Emission and Absorption in the 8-14 Micron Region", submitted and published in the *Proc. of the 12th Annual Astrophys. Symposium, Liege, Belgium. Contr. No. 1206, Div. Geol. Sciences, Cal Tech. (September 27, 1963)*.
- [35] Roberts, J. A., "Radio Emission From the Planets", *Planetary and Space Sciences*, 11, 221-229 (1963).
- [36] Burns, W. R., "Comparison of Perfect Finite Time Integrator and Dumped RC Smoothing Filter", internal correspondence (January 1964).

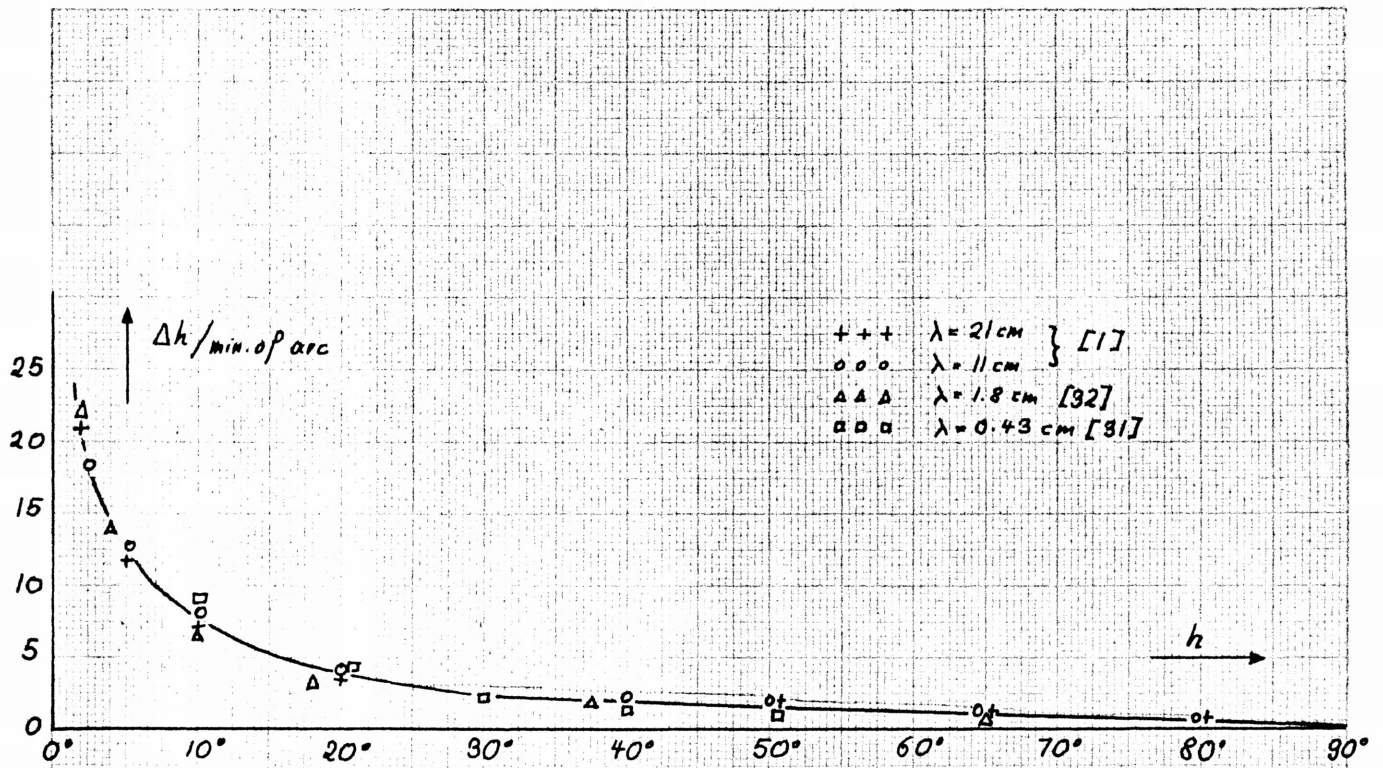


Fig. 1. Measured refraction at various wavelengths in the microwave region

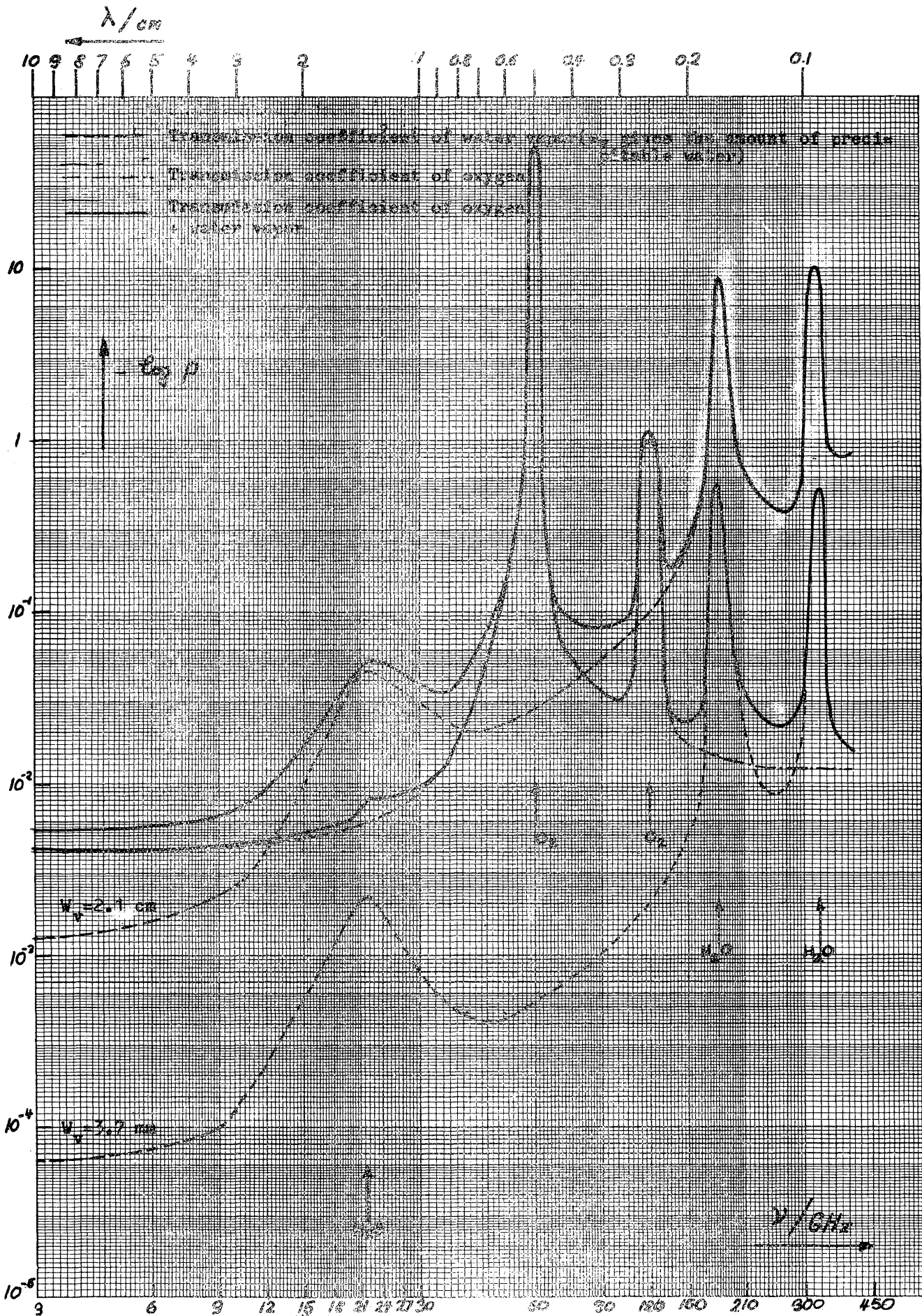


Fig. 2 : Calculated value of the zenith transmission coefficient of the atmosphere at Green Bank, WVA

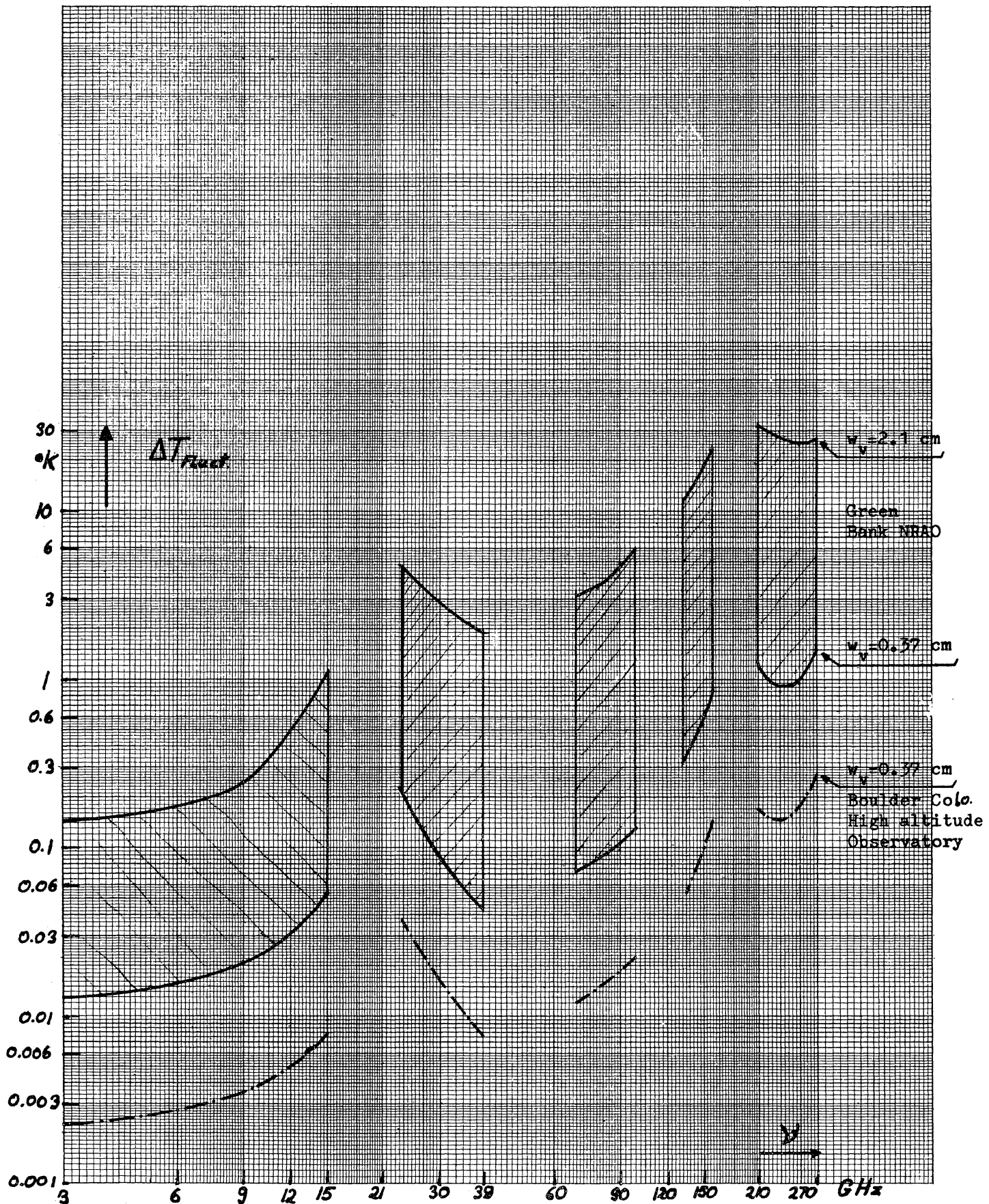


Fig.: 3 RMS Sky temperature fluctuations at good observing conditions (clear sky) for highest(2.1cm)and lowest(0.37cm)amount of precipitable water at Green Bank and Boulder.(estimated values)

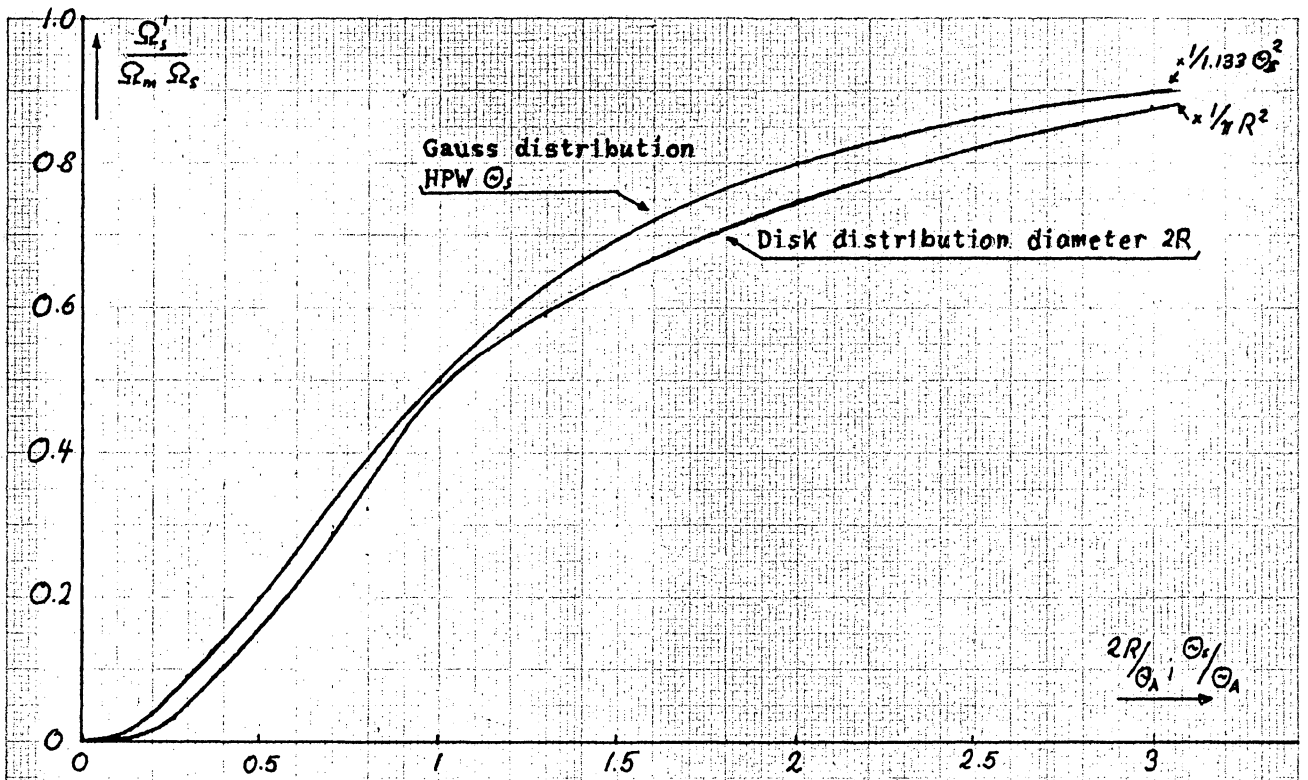


Fig.4a. The correction function eq.(11b) for the calculation of the flux density of extended radio sources. The Gauss- and the disk distribution are supposed to have the same HPW $2R = \Theta_s$

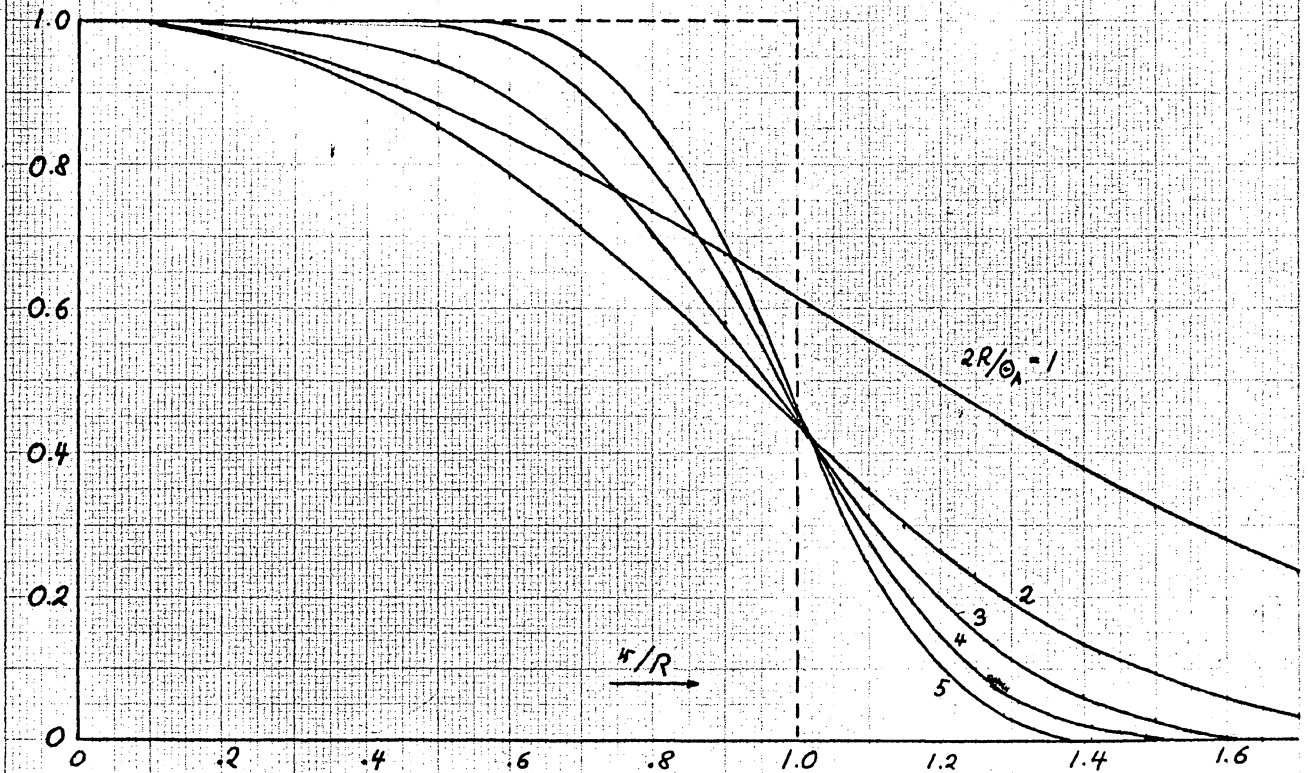


Fig.4b: Calculated drift curves of a gaussian antenna main beam with HPBW Θ_A with a disk of diameter $2R$ for various ratios $2R/\Theta_A$

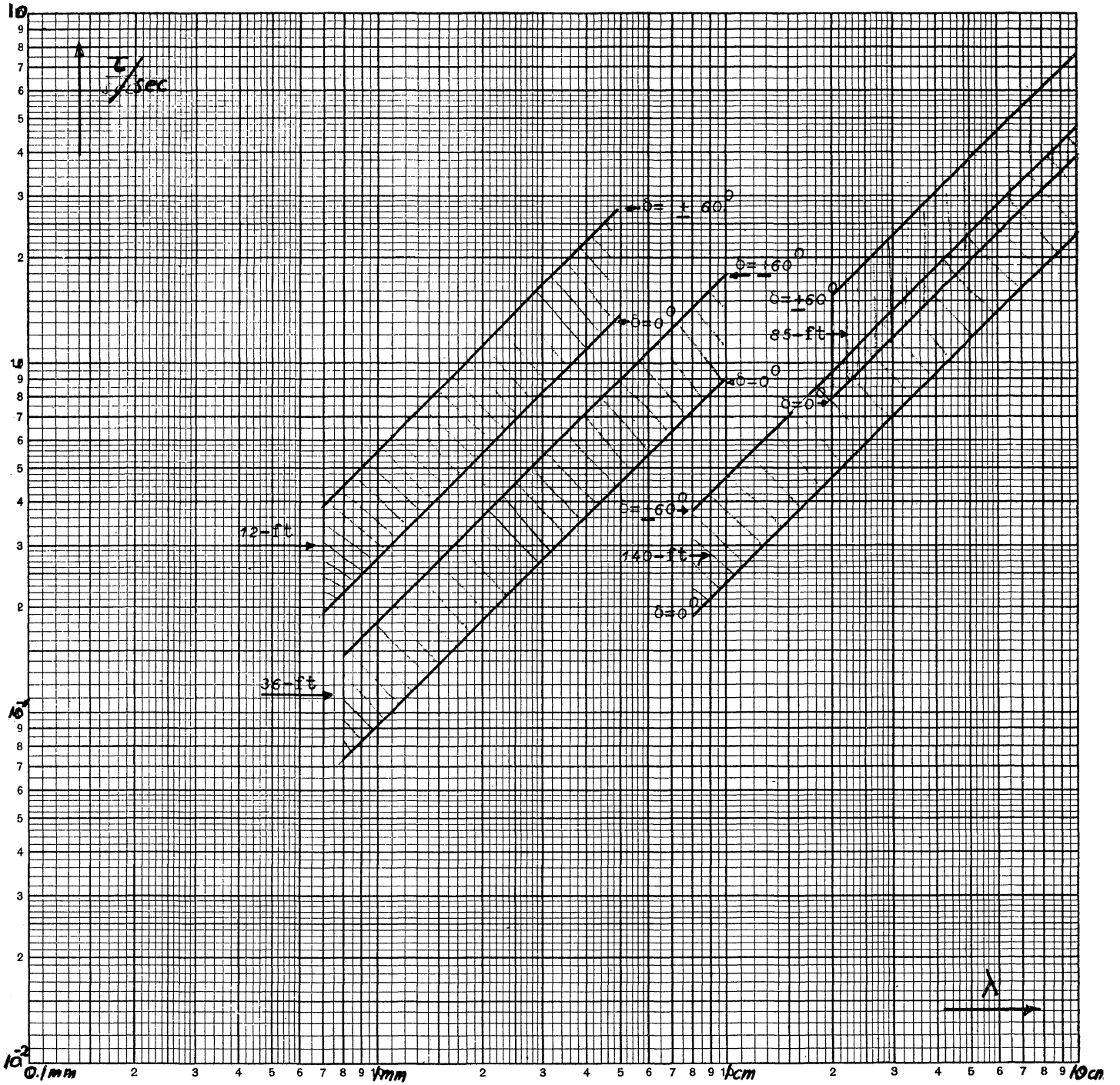


Fig.: 5 Range of time constants for the undistorted observation of point sources with different radio-telescopes

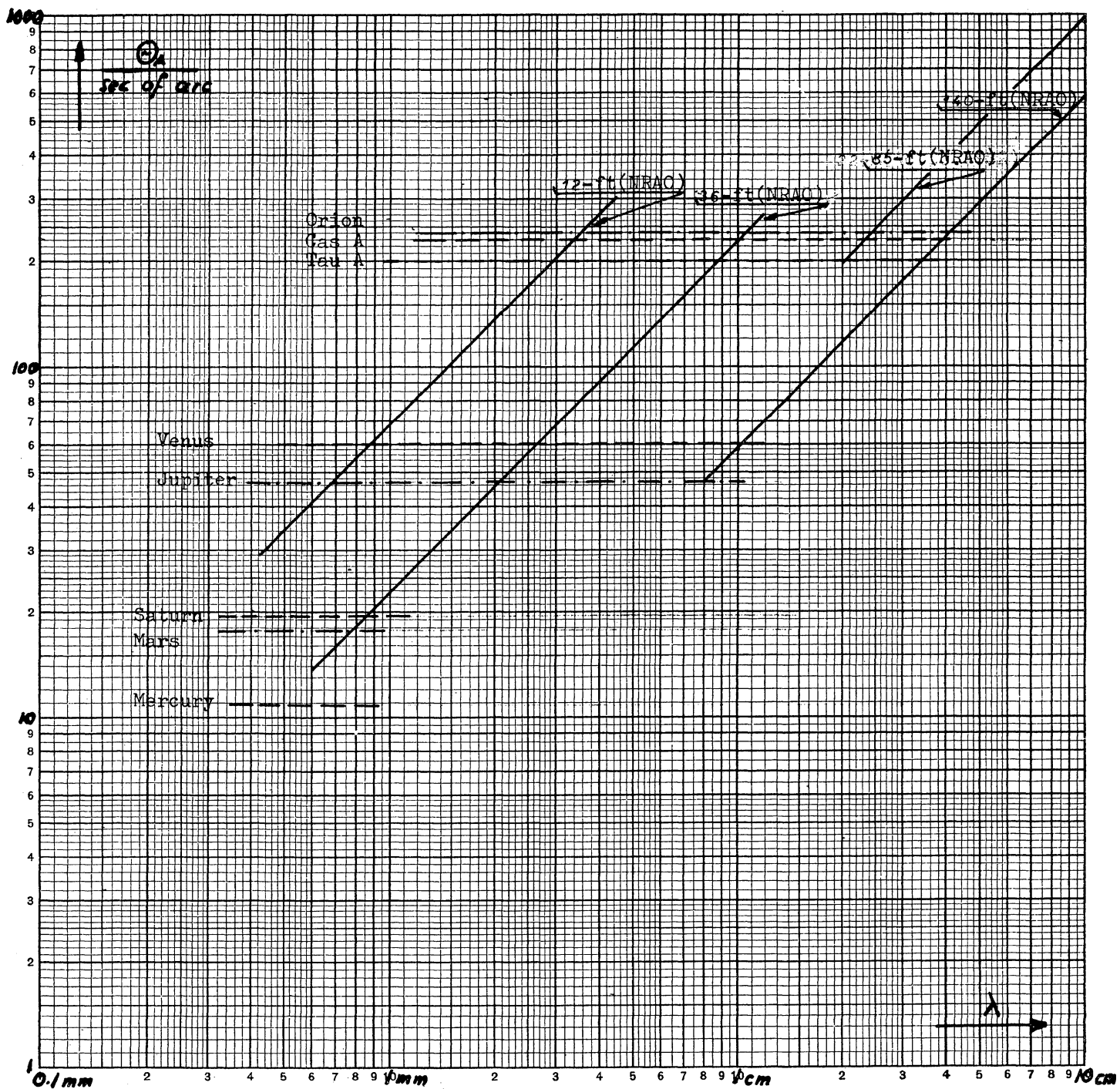


Fig. 6 HPBW of different antennas and apparent diameters of some radio sources

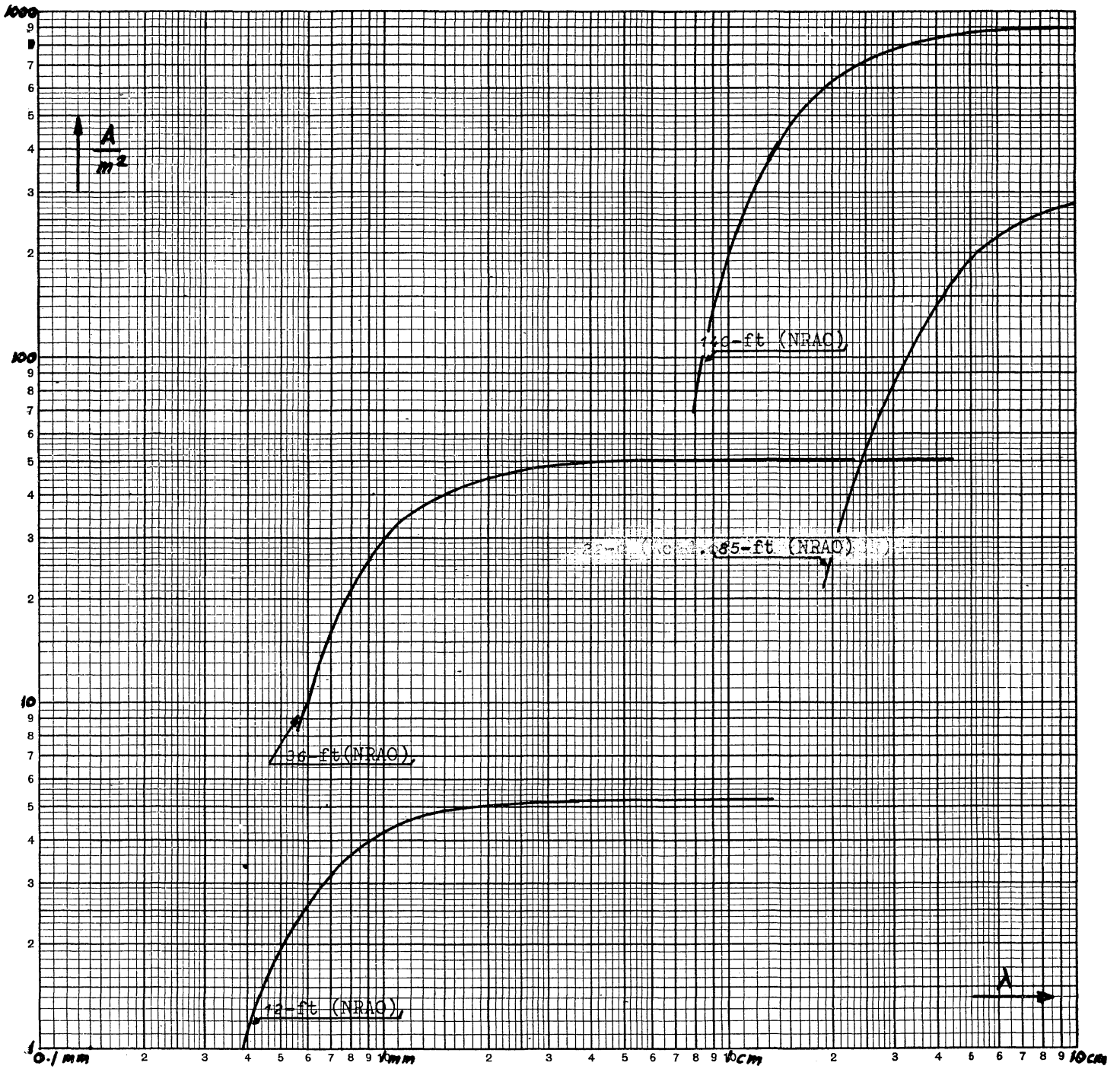


Fig.: 7 Effective areas of different antennas as a function of wavelength

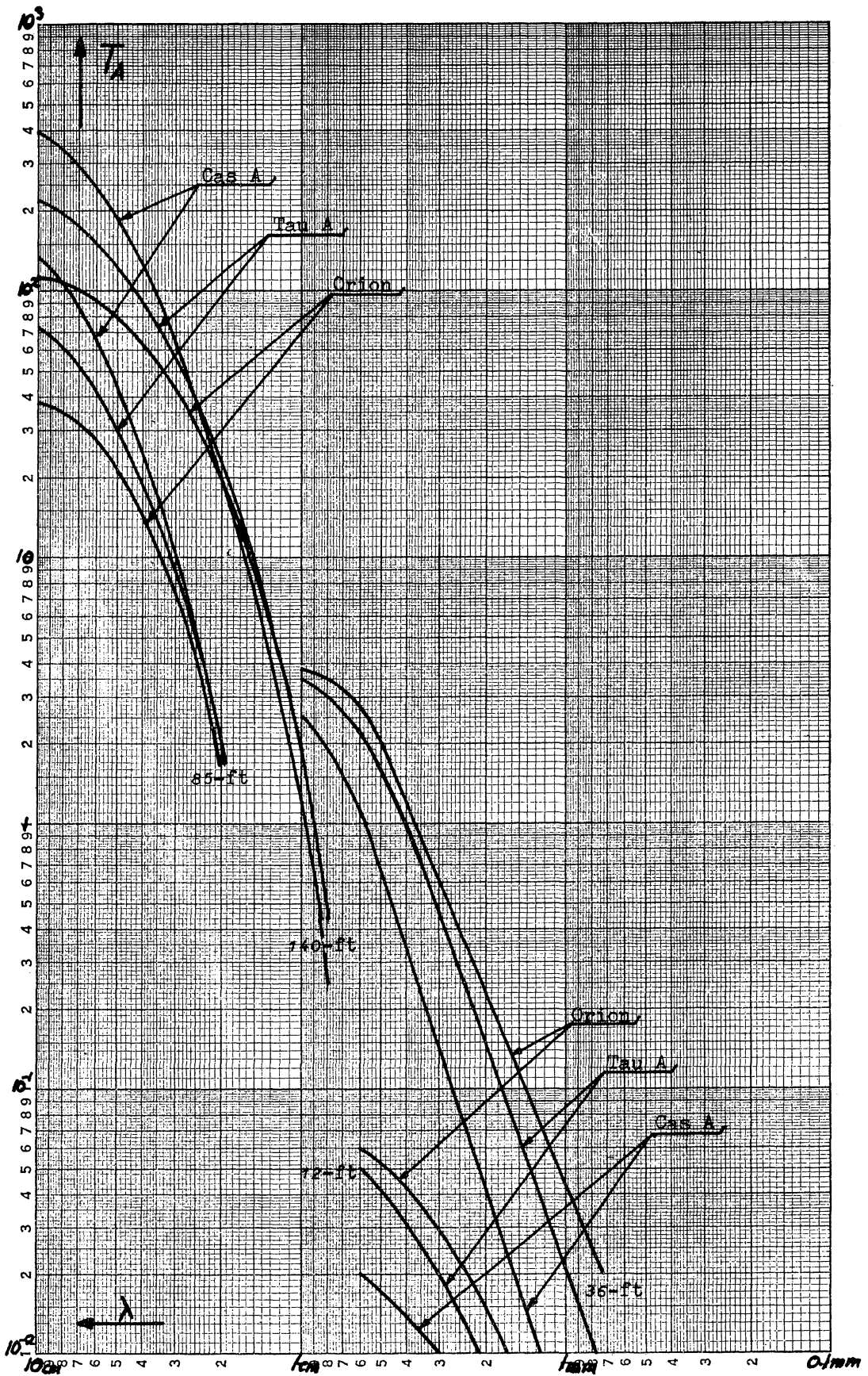


Fig.: 8 Expected antenna temperatures of Cas A, Tau A and Orion for the four NRAO antennas

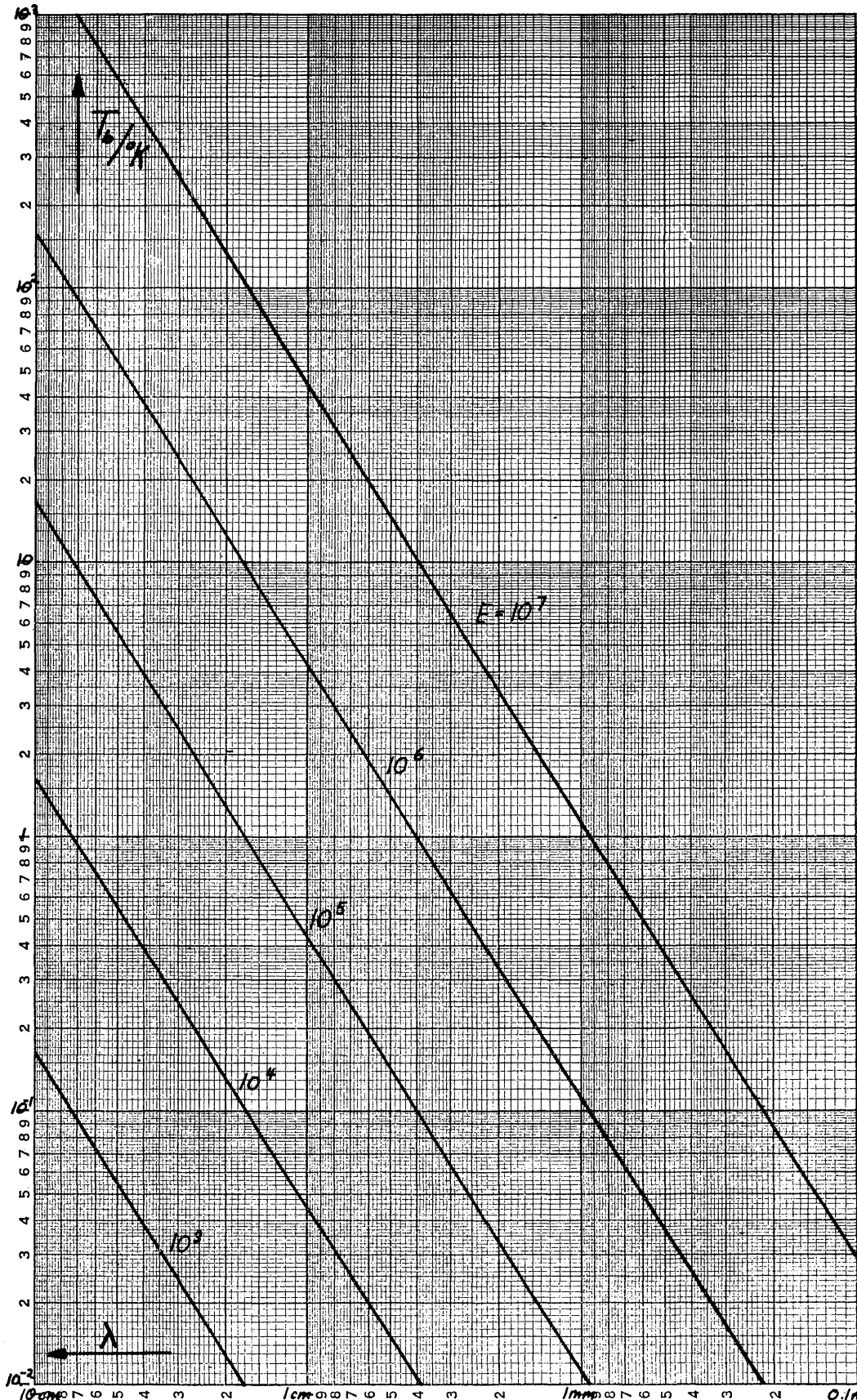


Fig.9: Radiation temperature of ~~non-opaque~~ ionized hydrogen ($T_e = 10^4$ °K) as a function of the wavelength
 Parameter is the emission measure E/cm^{-6} pc

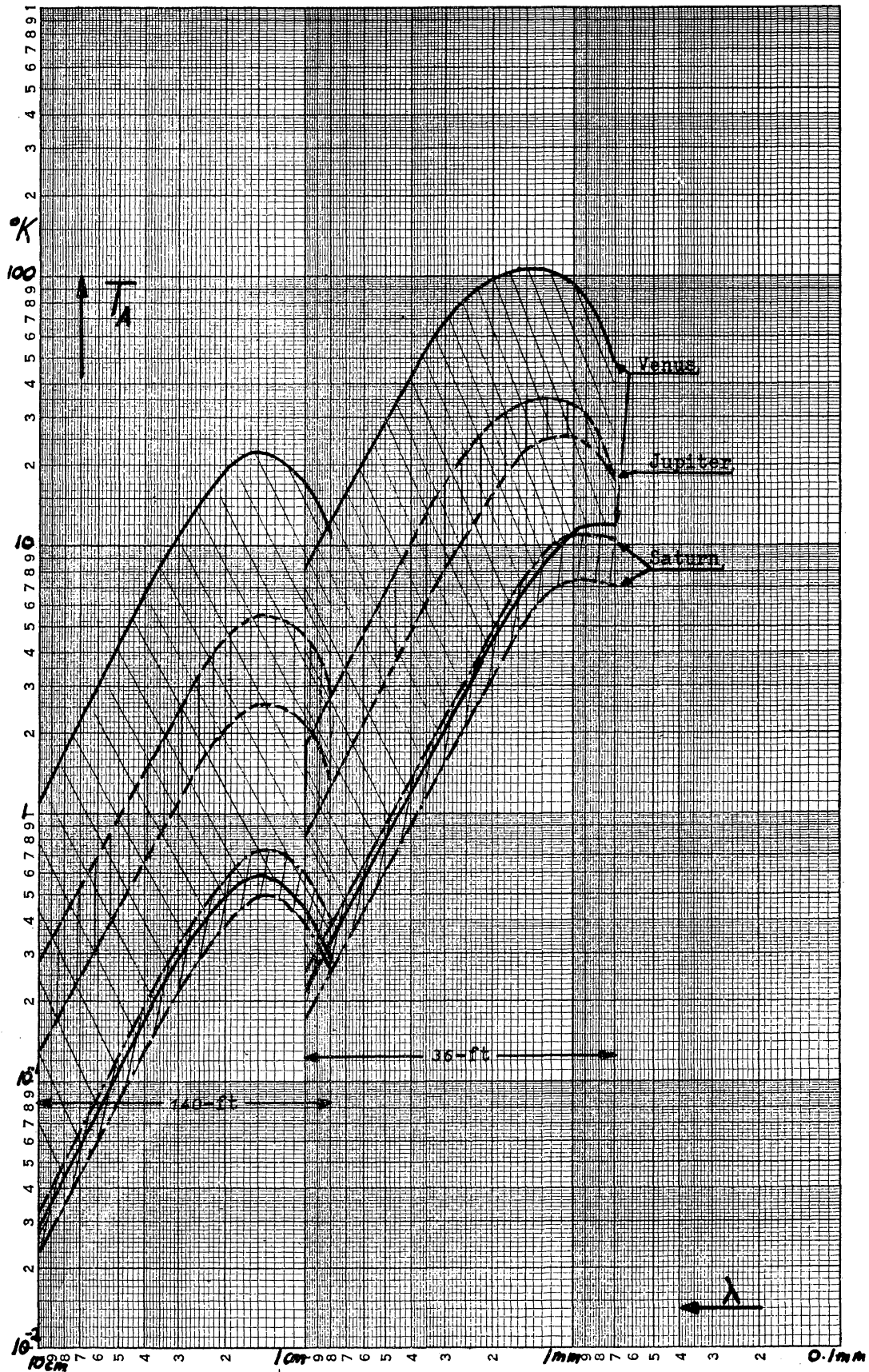


Fig. 10 : Antenna temperatures of some planets as a function of wavelength for the 140-ft and 36-ft antennas

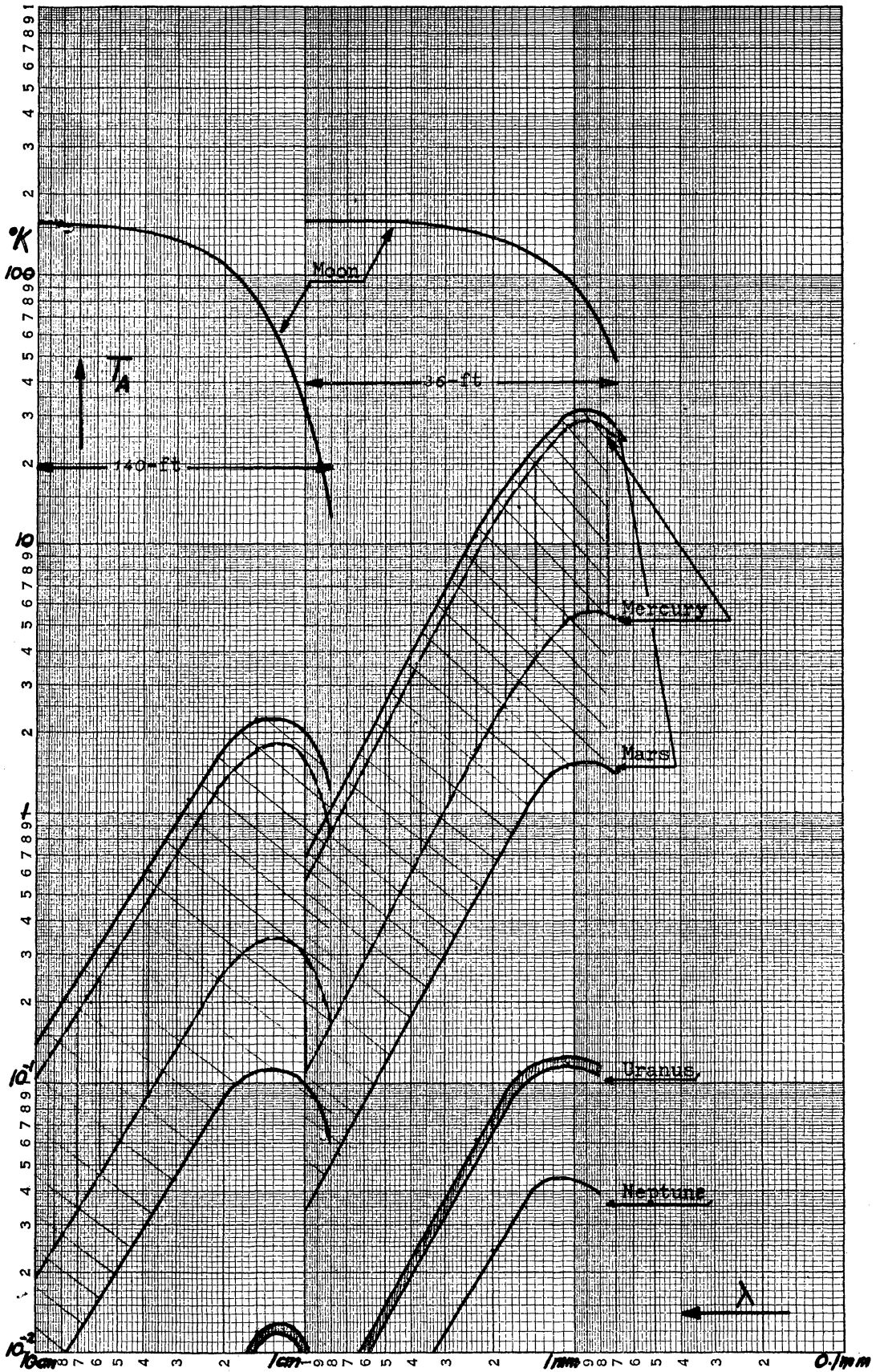


Fig. 11: Antenna temperature of the moon and of some planets as a function of wavelength for the 140-ft and the 36-ft antenna

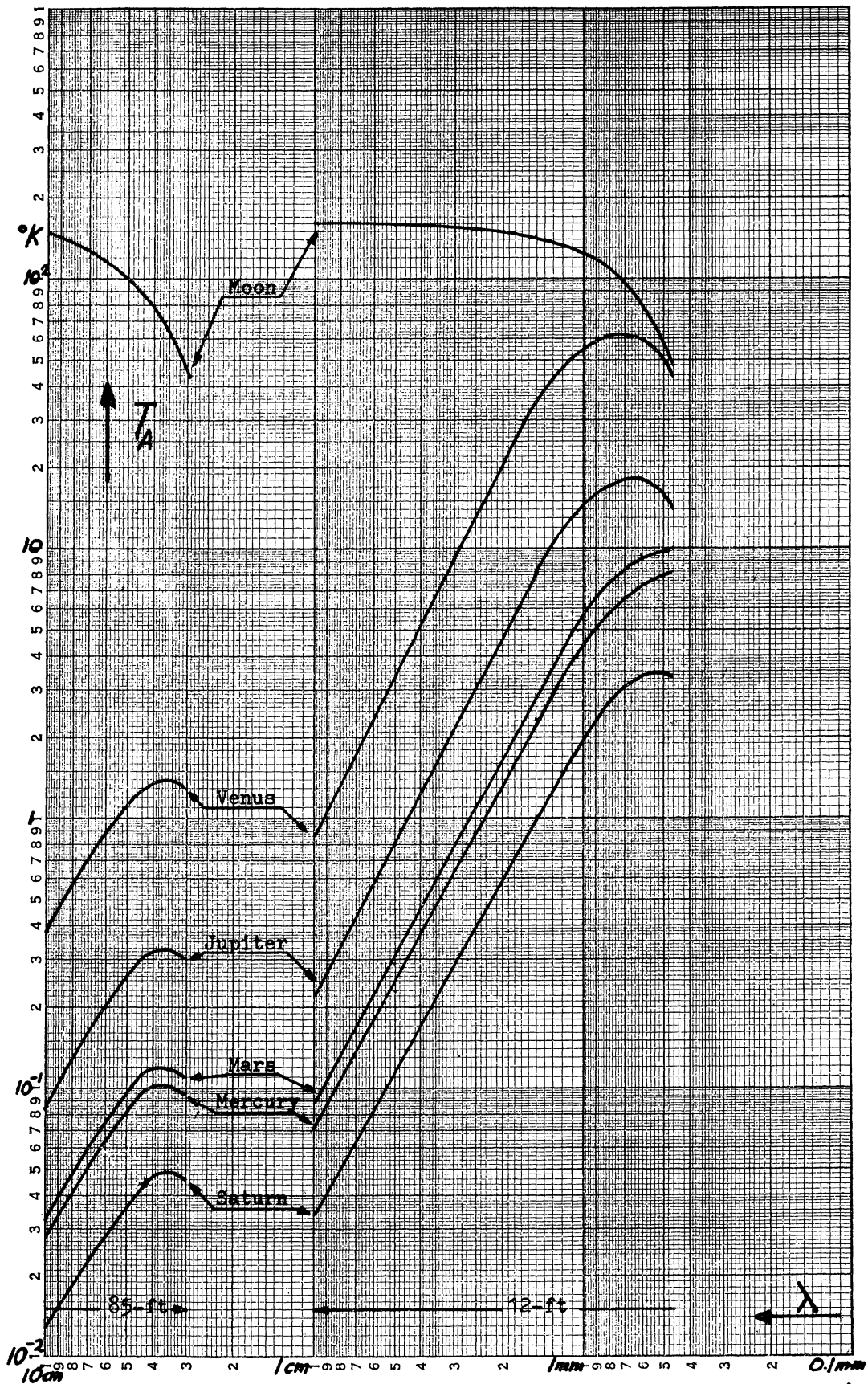


Fig. 12: Antenna temperatures of the moon (average temperatures) and of some planets (Maximum temperatures) for the 85-ft and the 12-ft antenna

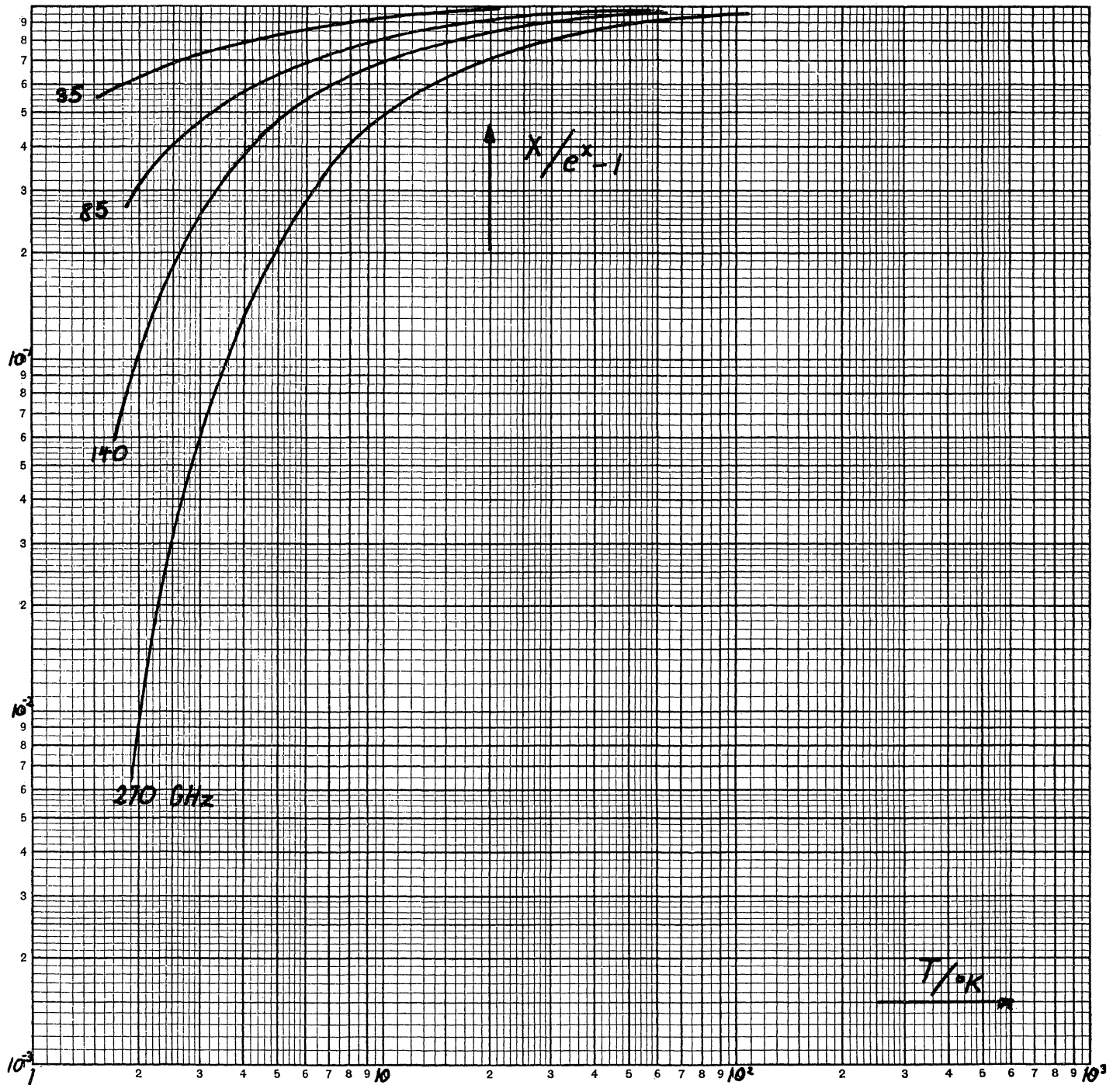


Fig.13: Deviation between Planck's law and the Rayleigh-Jeans approximation as a function of the radiation temperature T for the center frequencies in the four atmospheric windows in the mm-wave range

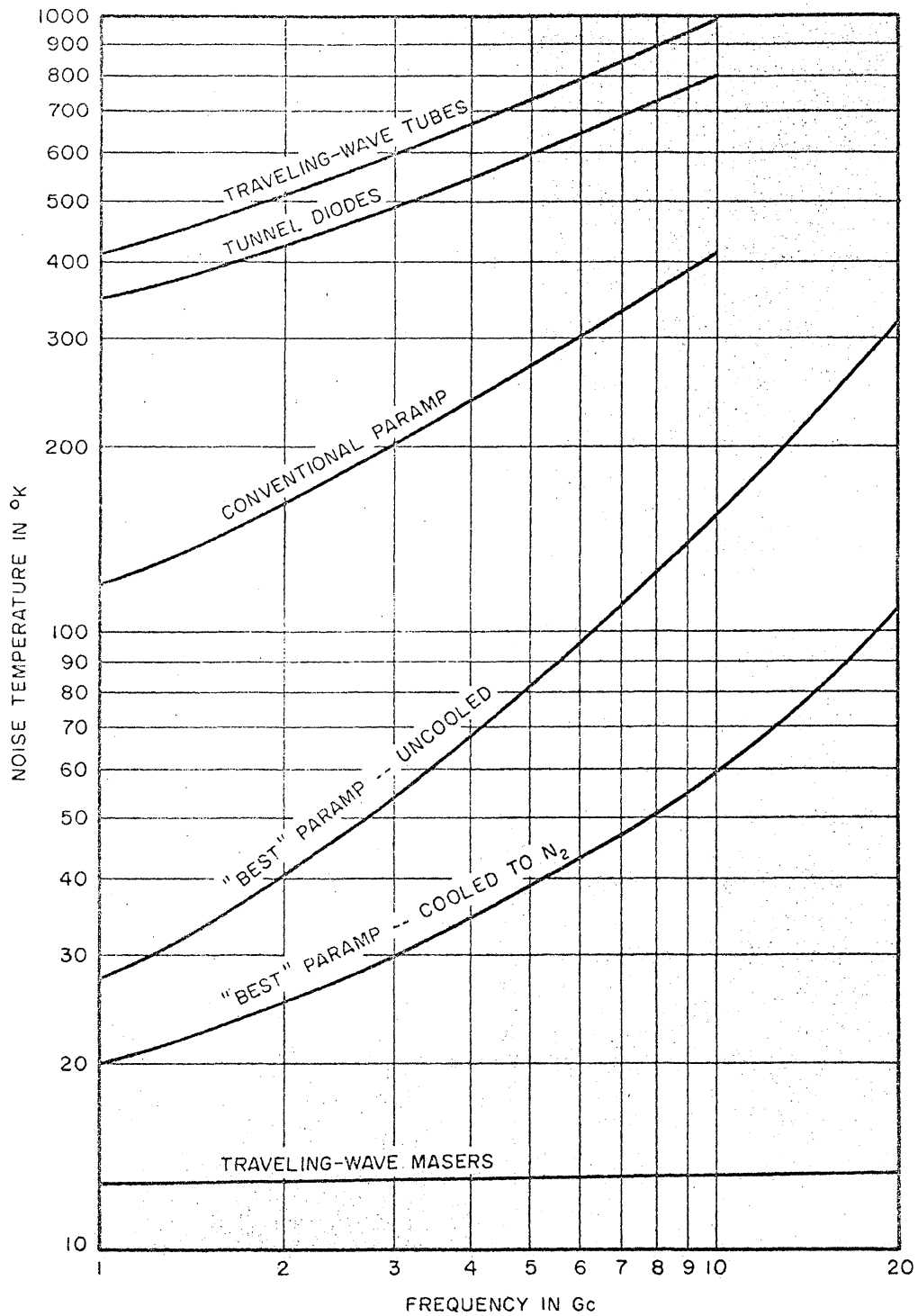


Fig. 14 NOISE TEMPERATURE OF VARIOUS RF AMPLIFIERS AS A FUNCTION OF OPERATING FREQUENCY
 (Prepared by **M. Lebenbaum**)

